Journal of Solid Mechanics Vol. 15, No. 4 (2023) pp. 402-427
DOI: 10.60664/jsm.2024.3051776

Research Paper

On The Aeroelastic Stability of A Two-Directional FG GNP-Enriched Conical Shell

A. Shahidi *, A. Darakhsh

Department of Mechanical Engineering, Isfahan University of Technology, 84156-83111, Isfahan, Iran

Received 12 May 2023; accepted 1 August 2023

ABSTRACT

In this article, the supersonic flutter analysis of a truncated conical shell made of polymer enriched with graphene nanoplatelets (GNPs) exposed to supersonic fluid flow is discussed. It is assumed that the mass fraction of the GNPs is functionally graded (FG) along thickness and length directions according to different dispersion patterns. Modeling of the shell is done using the first-order shear deformation theory (FSDT), the mechanical properties are computed according to the Halpin-Tsai model alongside the rule of the mixture, and the aerodynamic pressure is computed utilizing the piston theory. Utilizing Hamilton's principle, the boundary conditions and the governing equations are achieved. Harmonic trigonometric functions are used to provide an analytical solution in the circumferential direction and an approximate solution is presented in the meridional direction using the differential quadrature method (DQM). The efficacy of various parameters on the aeroelastic stability are discussed such as the percentage and dispersion pattern of the GNPs and gradient indices. It is observed that to achieve higher aeroelastic stability in the GNP-enriched truncated conical shells, it is better to dispense the GNPs near the small radius and the inner surface of the shell.

Keywords: Aeroelastic stability; Flutter analysis; Graphene nanoplatelets (GNPs); Two-directional functionally graded.

1 INTRODUCTION

CONICAL panels and shells have been utilized in the design of lots of parts in various industries associated with civil, aerospace, and mechanical engineering, such as high-speed centrifugal separators and the base of wind turbines. Due to the expanded range of usage and application of truncated conical shells in the aerospace industries, the aeroelastic stability and free vibration analyses of such structures are of high practical importance and have been examined in various experimental and analytical works. The vibrational (free and forced) characteristics of the truncated conical shells are extensively discussed by authors [1-5]. In comparison with the papers regarding the vibration analysis of the conical shells, there is a limited number of papers related to the flutter behavior of the

* Corresponding author. Tel.: +98 311 3915237; Fax: +98 311 3915216.
E-mail address: shahidi@cc.iau.ac.ir

conical shells. The authors' research shows that the initial works on the aeroelastic characteristics of the conical shells were provided in the 1970s including the experimental results provided by Miserentino [6] and the numerical ones provided via the finite element method (FEM) by Bismarck-Nasr and Savio [7]. Sunder et al. [8, 9] studied the aeroelastic stability of homogenous isotropic and 3-ply laminated truncated conical shells. It was observed by them that there is an optimum semi-vertex angle of the cone that brings about the highest aeroelastic stability. The flutter behavior of a partly fluid-filled truncated conical shell was discussed by Sabri et al. [10]. They reported that the internal pressure enhances the aeroelastic stability. Davar and Shokrollahi [11] studied the aeroelastic stability characteristics of FG conical panels. They concluded that the discrepancies between the classical shell theory (CPT) and the FSDT for the critical speed are remarkably greater than those for the natural frequencies. The relevance of the flutter boundaries of a truncated conical shell reinforced with carbon nanotubes (CNTs) to the hydrostatic pressure was examined by Mehri et al. [12]. It was discovered by them that the critical speed of the shell can be easily increased by increasing the volume fraction of the CNTs. Various shell theories were employed by Bakhtiari et al. [13] to examine the nonlinear flutter analysis of a conical shell. They discovered that geometrical nonlinearities in strain-deformation relations have a softening effect on the aeroelastic stability regions. Mahmoudkhani et al. [14] considered the temperature-dependent thermal and mechanical properties and investigated the aerothermoelastic stability behavior of an FG conical shell subjected to internal pressure in a thermal environment. It was concluded by them that internal pressure has a positive effect on aeroelastic stability, but temperature elevation has a negative effect on aeroelastic stability. Rahmanian and Javadi [15] studied the supersonic flutter analysis of a conical shell with arbitrary boundary conditions. It was observed by them that the critical aerodynamic pressure is more dependent on the boundary condition at the large edge of a conical shell than on the boundary condition at the small edge. Amirabadi et al. [16] examined the free vibration analysis of a spinning two-directional FG GNP-enriched conical shell. They discovered that to achieve higher natural frequencies, it is more beneficial to disperse the GNPs near the small radius and inner surface of the shell. The supersonic flutter characteristics of a three-phase laminated composite conical-conical shell made of polymeric epoxy enriched with GNPs and glass fibers were examined by Nasution et al. [17]. It was reported by them that a small growth in the percentage of the GNPs brings about significant growth in aeroelastic stability. Houshangi et al. [18] examined the aeroelastic stability of a sandwich conical shell with a magnetorheological elastomer (MR) core. It was discovered by them that the critical aerodynamic pressure can be raised by growing the density of the magnetic field. Amirabadi et al. [19] focused on the supersonic flutter behavior of a truncated conical shell with variable thickness. It was concluded by them that in order to enhance the aeroelastic stability of conical shells, it is more useful to raise the thickness from the small radius to the large one. Afshari et al. [20] provided a semi-analytical solution to examine the aeroelastic stability analysis of CNT-enriched polymeric truncated conical shell incorporating the CNTs agglomeration. It was observed by them that dispensing the CNTs near the inner and outer surfaces enhances the aeroelastic stability.

In Ref. [20], the impacts of nanofillers (CNTs) on the flutter behavior of a conical shell are discussed. In Ref. [20], it is supposed that the CNTs are dispersed based on various one-dimensional patterns along the thickness direction. To expand this research, the flutter behavior of a two-directional FG GNP-enriched truncated conical shell is studied in this paper for the first time. Investigating the flutter analysis of a truncated conical shell reinforced with two-directionally graded GNPs provides more general results. These results help designers and engineers to achieve better aeroelastic characteristics for GNP-reinforced conical shells used in future aerospace vehicles. Modeling of the shell is done utilizing the FSDT and modeling aerodynamic pressure provided by the external fluid flow is performed using the piston theory. The influences of several parameters on the flutter boundaries are investigated such as the dispersion pattern and mass fraction of the GNPs, gradient indices, the semi-vertex angle, and boundary conditions at both ends. The results of this work can be utilized to improve the design of structures in aerospace engineering to enhance the aeroelastic stability characteristics.

2 MATERIAL PROPERTIES

As schematically depicted in Figure 1, consider a truncated conical shell exposed to supersonic fluid flow of density ρ_∞ and velocity U_∞. The geometrical characteristics are thickness (h), semi-vertex angle (γ), length (L), small radius (a), and large radius (b).

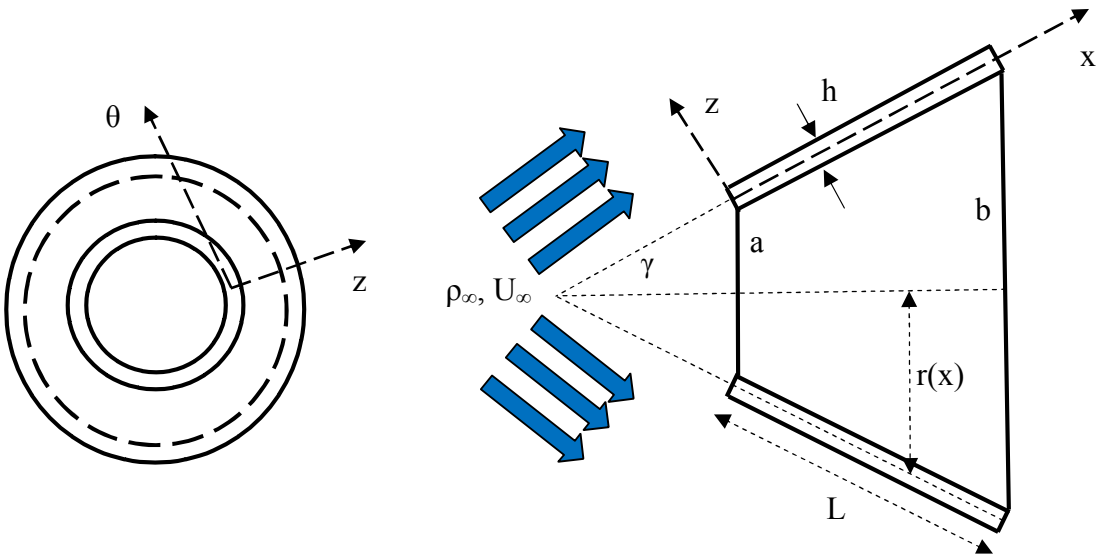

Fig.1
Geometrical parameters of a truncated conical shell subjected to fluid flow.

The shell is made of a matrix enriched with GNPs which are dispersed according to various patterns. The volume fractions of the GNPs (F_r) and the polymeric matrix (F_m) are presented as follows:

$$F_r(z,x) = F_r^* f(z,x), \quad F_m(z,x) = 1 - F_r(z,x), \tag{1}$$

where F^*_r is the total volume fraction of the GNPs which is related to the mass fraction of the GNPs (g^*_r) as [21]

$$F_r^* = \frac{g_r^*}{g_r^* + \frac{\rho_r}{\rho_m}\left(1 - g_r^*\right)}, \tag{2}$$

and $f(x,z)$ is considered for four selected dispersion patterns as follows [16]:

$$\begin{aligned}
&\text{Type 1:} \quad f(z,x) = (n_z+1)(n_x+1)\left(\frac{1}{2}+\frac{z}{h}\right)^{n_z}\left(\frac{x}{L}\right)^{n_x},\\
&\text{Type 2:} \quad f(z,x) = (n_z+1)(n_x+1)\left(\frac{1}{2}-\frac{z}{h}\right)^{n_z}\left(\frac{x}{L}\right)^{n_x},\\
&\text{Type 3:} \quad f(z,x) = \frac{(n_z+1)(n_x+1)}{n_x}\left(\frac{1}{2}+\frac{z}{h}\right)^{n_z}\left[1-\left(\frac{x}{L}\right)^{n_x}\right],\\
&\text{Type 4:} \quad f(z,x) = \frac{(n_z+1)(n_x+1)}{n_x}\left(\frac{1}{2}-\frac{z}{h}\right)^{n_z}\left[1-\left(\frac{x}{L}\right)^{n_x}\right],
\end{aligned} \tag{3}$$

in which n_x and n_z are gradient indices and for n_x=n_z=1, the GNPs dispersion patterns are shown in Figure 2, and the relevance of the dispersion pattern of the GNPs on the power-law indices for type 4 is shown in Figure 3.

It should be stated that to have a fair comparison between the dispersion patterns, Eq. (3) is regulated to result in the same value of the mass fraction (percentage) of the GNPs for all dispersion patterns. It can be checked using the relation below:

$$\frac{1}{Lh}\int_{-\frac{h}{2}}^{\frac{h}{2}}\int_{0}^{L} F_r(x,z)\,dxdz = F_r^*. \tag{4}$$

Employing the rule of mixture results in the relations below for the density (ρ) and the Poisson's ratio (ν) [22]:

$$\nu = F_m\nu_m + F_r\nu_r, \quad \rho = F_m\rho_m + F_r\rho_r, \tag{5}$$

in which, here and in what follows, the subscripts m and r respectively represent the matrix and the GNPs,

Utilizing the Halpin-Tsai model results in the relation below for the elastic modulus (E) of the shell [23]:

$$E=\left[\frac{3\left(1+F_r\xi_l\eta_l\right)}{1-F_r\eta_l}+\frac{5\left(1+F_r\xi_w\eta_w\right)}{1-F_r\eta_w}\right]\frac{E_m}{8}, \tag{6}$$

in which

$$\eta_l=\frac{\eta-1}{\eta+\xi_l},\quad \eta_w=\frac{\eta-1}{\eta+\xi_w},\quad \eta=\frac{E_r}{E_m},\quad \xi_l=\frac{2l_r}{h_r},\quad \xi_w=\frac{2w_r}{h_r}, \tag{7}$$

where h_r, l_r, w_r, and respectively show the thickness, length, and width of the GNPs.

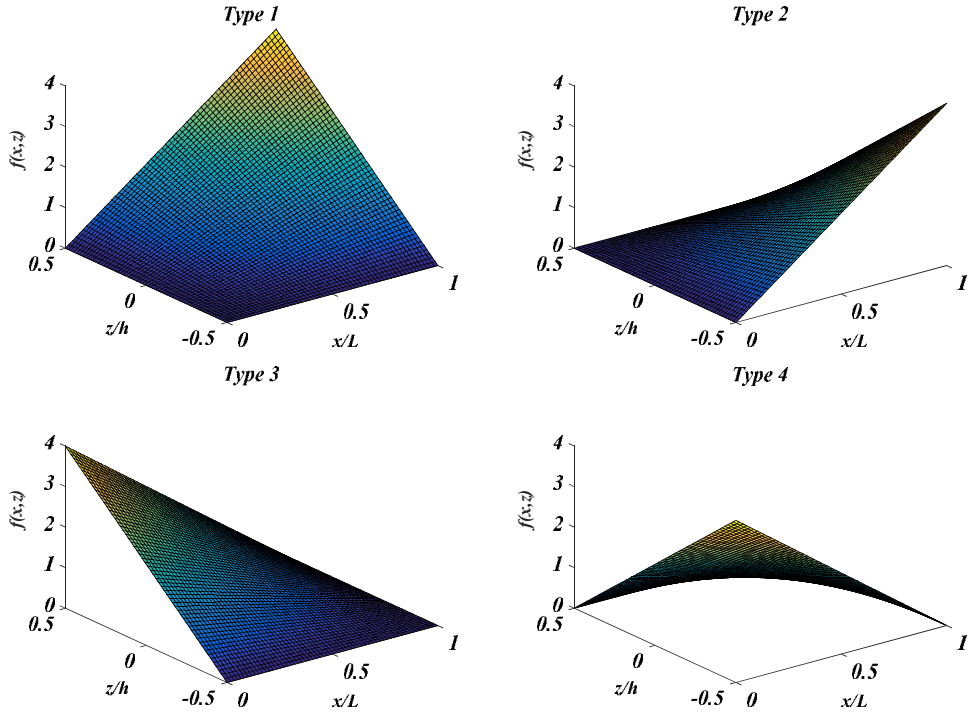

Fig.2
The GNPs dispersion patterns for n_x=n_z=1.

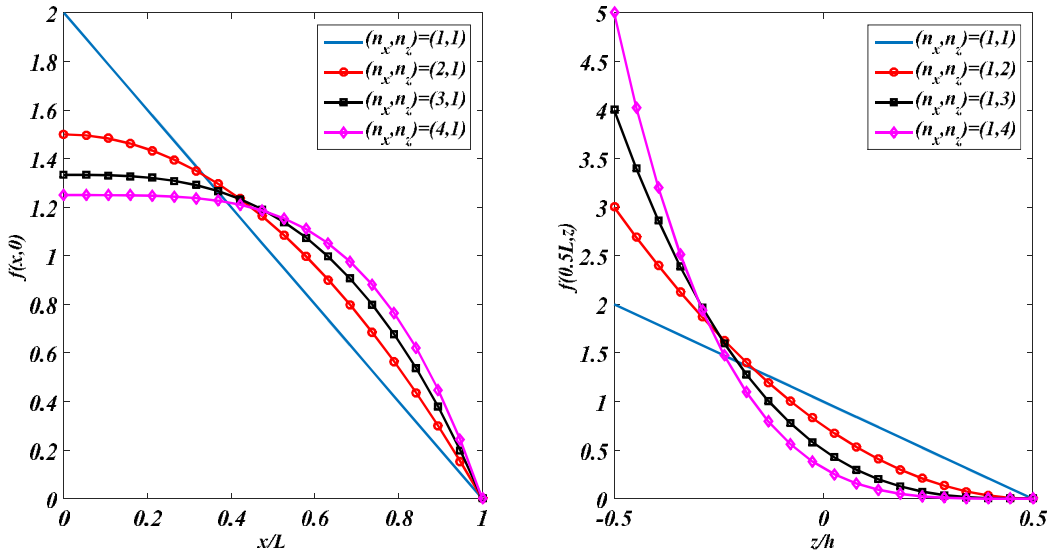

Fig.3
The effects of power-law indices on the dispersion pattern of GNPs for type 4.

3 DISPLACEMENT, STRAIN, STRESS

The oldest and simplest theories presented for shells are classical ones such as Donnell's, Flugge's, Love's, and Sanders' shell theories. In such theories, transverse components of stress tensor and rotational inertia are ignored and the corresponding results are reliable only for thin shells. In the FSDT, the transverse components of stress tensor and rotational inertia are included but the distributions of transverse components of stress tensor are not accurate enough. This shortage can be made up using the shear correction factor and the results obtained by this theory are reliable for both thin and moderately thick shells. It is noteworthy that to provide results reliable for thin, moderately thick, and thick shells, the higher-order shear deformation theories can be utilized which provide higher volumes of equations and computational efforts [4].

Utilizing the FSDT, the relations below can be used for the displacement field [24]:

$$\begin{aligned} u_1(t,z,\theta,x) &= u(t,\theta,x) + z\psi_x(t,\theta,x), \\ u_2(t,z,\theta,x) &= v(t,\theta,x) + z\psi_\theta(t,\theta,x), \\ u_3(t,z,\theta,x) &= w(t,\theta,x), \end{aligned} \tag{8}$$

in which u_1, u_2, and u_3 sequentially represent the displacement along *x, θ, and z* directions, and *u, v,* and *w* show the corresponding displacement in the middle surface of the shell.

The relations below provide the strain-displacement equations [25]:

$$\begin{aligned} \varepsilon_{xx} &= \frac{\partial u_1}{\partial x}, & 2\varepsilon_{\theta z} &= \frac{\partial u_2}{\partial z} - \frac{\cos\gamma}{r}u_2 + \frac{1}{r}\frac{\partial u_3}{\partial \theta}, \\ \varepsilon_{\theta\theta} &= \frac{\sin\gamma}{r}u_1 + \frac{1}{r}\frac{\partial u_2}{\partial \theta} + \frac{\cos\gamma}{r}u_3, & 2\varepsilon_{xz} &= \frac{\partial u_1}{\partial z} + \frac{\partial u_3}{\partial x}, \\ \varepsilon_{zz} &= \frac{\partial u_3}{\partial z}, & 2\varepsilon_{x\theta} &= \frac{1}{r}\frac{\partial u_1}{\partial \theta} + \frac{\partial u_2}{\partial x} - \frac{\sin\gamma}{r}u_2, \end{aligned} \tag{9}$$

where $r=a+x\sin\gamma$ stands for the radius of the shells.

Using Eqs. (8) and (9), the relations below are presented for the components of the strain:

$$\begin{Bmatrix} \varepsilon_{xx} \\ \varepsilon_{\theta\theta} \\ 2\varepsilon_{\theta z} \\ 2\varepsilon_{xz} \\ 2\varepsilon_{x\theta} \end{Bmatrix} = \begin{Bmatrix} \dfrac{\partial u}{\partial x} \\ \dfrac{1}{r}\left(u\sin\gamma + \dfrac{\partial v}{\partial \theta} + w\cos\gamma\right) \\ \psi_\theta + \dfrac{1}{r}\left(\dfrac{\partial w}{\partial \theta} - v\cos\gamma\right) \\ \psi_x + \dfrac{\partial w}{\partial x} \\ \dfrac{\partial v}{\partial x} - \dfrac{1}{r}\left(v\sin\gamma - \dfrac{\partial u}{\partial \theta}\right) \end{Bmatrix} + z\begin{Bmatrix} \dfrac{\partial \psi_x}{\partial x} \\ \dfrac{1}{r}\left(\psi_x\sin\gamma + \dfrac{\partial \psi_\theta}{\partial \theta}\right) \\ 0 \\ 0 \\ \dfrac{\partial \psi_\theta}{\partial x} + \dfrac{1}{r}\left(\dfrac{\partial \psi_x}{\partial \theta} - \psi_\theta\sin\gamma\right) \end{Bmatrix} \tag{10}$$

The following stress-strain relations can be utilized for the isotropic shell:

$$\begin{Bmatrix} \sigma_{xx} \\ \sigma_{\theta\theta} \\ \sigma_{\theta z} \\ \sigma_{xz} \\ \sigma_{x\theta} \end{Bmatrix} = \begin{bmatrix} C_{11} & C_{12} & 0 & 0 & 0 \\ C_{21} & C_{22} & 0 & 0 & 0 \\ 0 & 0 & k_s C_{44} & 0 & 0 \\ 0 & 0 & 0 & k_s C_{55} & 0 \\ 0 & 0 & 0 & 0 & C_{66} \end{bmatrix} \begin{Bmatrix} \varepsilon_{xx} \\ \varepsilon_{\theta\theta} \\ 2\varepsilon_{\theta z} \\ 2\varepsilon_{xz} \\ 2\varepsilon_{x\theta} \end{Bmatrix}, \tag{11}$$

where the shear correction factor is k_s=5/6 and

$$C_{11} = C_{22} = \frac{E}{1-\nu^2}, \quad C_{12} = C_{21} = \nu C_{11}, \quad C_{44} = C_{55} = C_{66} = \frac{E}{2(1+\nu)}. \tag{12}$$

4 GOVERNING EQUATIONS

The relation below provides the governing equations along with the boundary conditions for the dynamic analysis of a structure:

$$\int_{t_1}^{t_2} \delta\left(T_s + W_{n.c.} - U_s\right) dt = 0, \tag{13}$$

which is known as Hamilton's principle, where δ is called the variational operator, t is time, t_1 and t_2 are two arbitrary moments, and T_s, $W_{n.c.}$, and U_s respectively represent the kinetic energy, the work done by non-conservative loads, and the strain energy.

The relation below provides the variation of the kinetic energy:

$$\delta T_s = \iiint_V \rho\left(\frac{\partial u_1}{\partial t}\frac{\partial \delta u_1}{\partial t} + \frac{\partial u_2}{\partial t}\frac{\partial \delta u_2}{\partial t} + \frac{\partial u_3}{\partial t}\frac{\partial \delta u_3}{\partial t}\right) dV, \tag{14}$$

in which V stands for the volume ($dv=dzdS$), and dS shows the surface of the shell ($dS=rdxd\theta$).

Utilizing Eqs. (8) and (14), the kinetic energy is represented as follows:

$$\begin{aligned}\delta T_s = \iint_S \Bigg[& J_0\left(\frac{\partial \delta u}{\partial t}\frac{\partial u}{\partial t} + \frac{\partial \delta v}{\partial t}\frac{\partial v}{\partial t} + \frac{\partial \delta w}{\partial t}\frac{\partial w}{\partial t}\right) + J_1\left(\frac{\partial \delta \psi_x}{\partial t}\frac{\partial u}{\partial t} + \frac{\partial \delta u}{\partial t}\frac{\partial \psi_x}{\partial t} + \frac{\partial \delta \psi_\theta}{\partial t}\frac{\partial v}{\partial t} + \frac{\partial \delta v}{\partial t}\frac{\partial \psi_\theta}{\partial t}\right) \\ & + J_2\left(\frac{\partial \delta \psi_x}{\partial t}\frac{\partial \psi_x}{\partial t} + \frac{\partial \delta \psi_\theta}{\partial t}\frac{\partial \psi_\theta}{\partial t}\right)\Bigg] dS,\end{aligned} \tag{15}$$

in which

$$\begin{Bmatrix} J_0(x) \\ J_1(x) \\ J_2(x) \end{Bmatrix} = \int_{-\frac{h}{2}}^{\frac{h}{2}} \begin{Bmatrix} 1 \\ z \\ z^2 \end{Bmatrix} \rho(x,z)\, dz. \tag{16}$$

The relation below provides the variation of the strain energy:

$$\delta U_s = \iiint_V \left[\sigma_{xx}\delta\varepsilon_{xx} + \sigma_{\theta\theta}\delta\varepsilon_{\theta\theta} + 2\left(\sigma_{xz}\delta\varepsilon_{xz} + \sigma_{\theta z}\delta\varepsilon_{\theta z} + \sigma_{x\theta}\delta\varepsilon_{x\theta}\right)\right] dV, \tag{17}$$

which can be represented using Eq. (10) as

$$\begin{aligned}\delta U_s = \iint_S \Bigg[& N_{xx}\frac{\partial \delta u}{\partial x} + M_{xx}\frac{\partial \delta \psi_x}{\partial x} + \frac{N_{\theta\theta}}{r}\left(\delta u \sin\gamma + \delta w \cos\gamma + \frac{\partial \delta v}{\partial \theta}\right) + \frac{M_{\theta\theta}}{r}\left(\frac{\partial \delta \psi_\theta}{\partial \theta} + \delta\psi_x \sin\gamma\right) \\ & + N_{x\theta}\left(\frac{1}{r}\frac{\partial \delta u}{\partial \theta} - \frac{\sin\gamma}{r}\delta v + \frac{\partial \delta v}{\partial x}\right) + M_{x\theta}\left(\frac{\partial \delta \psi_\theta}{\partial x} + \frac{1}{r}\frac{\partial \delta \psi_x}{\partial \theta} - \frac{\delta\psi_\theta}{r}\sin\gamma\right) \\ & + Q_{xz}\left(\delta\psi_x + \frac{\partial \delta w}{\partial x}\right) + Q_{\theta z}\left(-\frac{\cos\gamma}{r}\delta v + \frac{1}{r}\frac{\partial \delta w}{\partial \theta} + \delta\psi_\theta\right)\Bigg] dS,\end{aligned} \tag{18}$$

where

$$\begin{Bmatrix} N_{xx} \\ N_{\theta\theta} \\ N_{x\theta} \end{Bmatrix} = \int_{-\frac{h}{2}}^{\frac{h}{2}} \begin{Bmatrix} \sigma_{xx} \\ \sigma_{\theta\theta} \\ \sigma_{x\theta} \end{Bmatrix} dz, \quad \begin{Bmatrix} Q_{xz} \\ Q_{\theta z} \end{Bmatrix} = \int_{-\frac{h}{2}}^{\frac{h}{2}} \begin{Bmatrix} \sigma_{xz} \\ \sigma_{\theta z} \end{Bmatrix} dz, \quad \begin{Bmatrix} M_{xx} \\ M_{\theta\theta} \\ M_{x\theta} \end{Bmatrix} = \int_{-\frac{h}{2}}^{\frac{h}{2}} \begin{Bmatrix} \sigma_{xx} \\ \sigma_{\theta\theta} \\ \sigma_{x\theta} \end{Bmatrix} z\, dz, \tag{19}$$

which can be presented utilizing Eqs. (10) and (11) as follows:

$$\begin{Bmatrix} N_{xx} \\ N_{\theta\theta} \\ M_{xx} \\ M_{\theta\theta} \end{Bmatrix} = \begin{bmatrix} A_{11} & A_{12} & B_{11} & B_{12} \\ A_{12} & A_{22} & B_{12} & B_{22} \\ B_{11} & B_{12} & D_{11} & D_{12} \\ B_{12} & B_{22} & D_{12} & D_{22} \end{bmatrix} \begin{Bmatrix} \dfrac{\partial u}{\partial x} \\ \dfrac{1}{r}\left(u\sin\gamma + \dfrac{\partial v}{\partial \theta} + w\cos\gamma\right) \\ \dfrac{\partial \psi_x}{\partial x} \\ \dfrac{1}{r}\left(\psi_x \sin\gamma + \dfrac{\partial \psi_\theta}{\partial \theta}\right) \end{Bmatrix}, \tag{20}$$

$$\begin{Bmatrix} N_{x\theta} \\ M_{x\theta} \end{Bmatrix} = \begin{bmatrix} A_{66} & A_{66} & B_{66} & B_{66} \\ B_{66} & B_{66} & D_{66} & D_{66} \end{bmatrix} \begin{Bmatrix} \dfrac{\partial v}{\partial x} \\ \dfrac{1}{r}\left(\dfrac{\partial u}{\partial \theta} - v\sin\gamma\right) \\ \dfrac{\partial \psi_\theta}{\partial x} \\ \dfrac{1}{r}\left(\dfrac{\partial \psi_x}{\partial \theta} - \psi_\theta \sin\gamma\right) \end{Bmatrix}, \quad \begin{Bmatrix} Q_{xz} \\ Q_{\theta z} \end{Bmatrix} = k_s \begin{bmatrix} A_{55} & 0 \\ 0 & A_{44} \end{bmatrix} \begin{Bmatrix} \dfrac{\partial w}{\partial x} + \psi_x \\ \dfrac{1}{r}\dfrac{\partial w}{\partial \theta} - \dfrac{\cos\gamma}{r} v + \psi_\theta \end{Bmatrix}.$$

where

$$\begin{Bmatrix} A_{ij}(x) \\ B_{ij}(x) \\ D_{ij}(x) \end{Bmatrix} = \int_{-\frac{h}{2}}^{\frac{h}{2}} \begin{Bmatrix} 1 \\ z \\ z^2 \end{Bmatrix} C_{ij}(z,x)\, dz, \quad i,j = 1,2,4,5,6. \tag{21}$$

As stated, the shell is exposed to the aerodynamic pressure (p) created by the external supersonic fluid flow. The relation below provides the variation of the work (virtual work) done by this non-conservative load:

$$\delta W_{n.c.} = \iint_S p\,\delta w\, dS. \tag{22}$$

According to the piston theory and by neglecting the aerodynamic damping, the relation below provides the aerodynamic pressure [26, 27]:

$$p(x,\theta,t) = \frac{\eta}{2r} w - \xi \frac{\partial w}{\partial x}, \tag{23}$$

in which

$$\eta = \rho_\infty U_0^2 M_\infty^2 \left(M_\infty^2 - 1\right)^{-1}, \quad \xi = \rho_\infty U_0^2 M_\infty^2 \left(M_\infty^2 - 1\right)^{-\frac{1}{2}}, \tag{24}$$

where $M_\infty = U_\infty / U_0$ is the well-known Mach number and U_0 is the velocity of sound. In Eqs. (23) and (24), ξ is known as the aerodynamic pressure coefficient and plays the dominant role in the instability of a structure exposed to supersonic fluid flow. Also, η incorporates the effect of the curvature of the structure and is not as effective as the aerodynamic pressure coefficient in determining the flutter boundaries [28].

Substituting Eqs. (15), (18), and (22) into Hamilton's principle provides the relations below as the governing equations:

$$\begin{aligned}
&\frac{\partial N_{xx}}{\partial x} + \frac{\sin\gamma}{r}\left(N_{xx} - N_{\theta\theta}\right) + \frac{1}{r}\frac{\partial N_{x\theta}}{\partial \theta} - J_0 \frac{\partial^2 u}{\partial t^2} - J_1 \frac{\partial^2 \psi_x}{\partial t^2} = 0, \\
&\frac{1}{r}\frac{\partial N_{\theta\theta}}{\partial \theta} + \frac{2\sin\gamma}{r} N_{x\theta} + \frac{\cos\gamma}{r} Q_{\theta z} + \frac{\partial N_{x\theta}}{\partial x} - J_0 \frac{\partial^2 v}{\partial t^2} - J_1 \frac{\partial^2 \psi_\theta}{\partial t^2} = 0, \\
&-\frac{\cos\gamma}{r} N_{\theta\theta} + \frac{\partial Q_{xz}}{\partial x} + \frac{\sin\gamma}{r} Q_{xz} + \frac{1}{r}\frac{\partial Q_{\theta z}}{\partial \theta} - J_0 \frac{\partial^2 w}{\partial t^2} + p = 0, \\
&\frac{\partial M_{xx}}{\partial x} + \frac{\sin\gamma}{r}\left(M_{xx} - M_{\theta\theta}\right) + \frac{1}{r}\frac{\partial M_{x\theta}}{\partial \theta} - Q_{xz} - J_1 \frac{\partial^2 u}{\partial t^2} - J_2 \frac{\partial^2 \psi_x}{\partial t^2} = 0, \\
&\frac{1}{r}\frac{\partial M_{\theta\theta}}{\partial \theta} + \frac{\partial M_{x\theta}}{\partial x} + \frac{2\sin\gamma}{r} M_{x\theta} - Q_{\theta z} - J_1 \frac{\partial^2 v}{\partial t^2} - J_2 \frac{\partial^2 \psi_\theta}{\partial t^2} = 0,
\end{aligned} \tag{25}$$

and the relations below as the boundary conditions:

$$\begin{aligned}
&\text{Clamped } (\mathrm{C}): \quad u = v = w = 0, \quad \psi_x = \psi_\theta = 0, \\
&\text{Simply supported } (\mathrm{S}): \quad v = w = 0, \quad \psi_\theta = 0, \quad N_{xx} = 0, \quad M_{xx} = 0, \\
&\text{Free } (\mathrm{F}): \quad N_{xx} = N_{x\theta} = Q_{xz} = 0, \quad M_{xx} = M_{x\theta} = 0.
\end{aligned} \tag{26}$$

By substituting Eqs. (20) and (23) into the governing equations (Eq. (25)) and employing the following solutions [29]:

$$\left\{\begin{matrix} u(t,\theta,x) \\ w(t,\theta,x) \\ \psi_x(t,\theta,x) \end{matrix}\right\} = \left\{\begin{matrix} U(x) \\ W(x) \\ X(x) \end{matrix}\right\} e^{\omega t}\cos(m\theta), \qquad m = 0,1,2,3,\ldots \tag{27}$$
$$\left\{\begin{matrix} v(t,\theta,x) \\ \psi_\theta(t,\theta,x) \end{matrix}\right\} = \left\{\begin{matrix} V(x) \\ \Theta(x) \end{matrix}\right\} e^{\omega t}\sin(m\theta),$$

in which ω is an eigenvalue and m is known as the circumferential wave number, the following set of governing equations can be obtained:

$$\begin{aligned}
&-\omega^2\left(J_0U + J_1X\right) + A_{11}U'' + \left(A'_{11} + A_{11}r^{-1}\sin\gamma\right)U' + \left[A'_{12}r^{-1}\sin\gamma - \left(A_{22}\sin^2\gamma + A_{66}m^2\right)r^{-2}\right]U \\
&+m\left(A_{12}+A_{66}\right)r^{-1}V' + m\left[A'_{12}r^{-1} - \left(A_{22}+A_{66}\right)r^{-2}\sin\gamma\right]V + A_{12}r^{-1}\cos\gamma W' \\
&+\cos\gamma\left(A'_{12}r^{-1} - A_{22}r^{-2}\sin\gamma\right)W + B_{11}X'' + \left(B'_{11} + B_{11}r^{-1}\sin\gamma\right)X' \\
&+\left[B'_{12}r^{-1}\sin\gamma - \left(B_{22}\sin^2\gamma + B_{66}m^2\right)r^{-2}\right]X + m\left(B_{12}+B_{66}\right)r^{-1}\Theta' + m\left[B'_{12}r^{-1} - \left(B_{22}+B_{66}\right)r^{-2}\sin\gamma\right]\Theta = 0, \\
&-\omega^2\left(J_0V + J_1\Theta\right) - m\left(A_{12}+A_{66}\right)r^{-1}U' - m\left[A'_{66}r^{-1} + \left(A_{22}+A_{66}\right)r^{-2}\sin\gamma\right]U + A_{66}V'' \\
&+\left(A'_{66} + A_{66}r^{-1}\sin\gamma\right)V' - \left[A'_{66}r^{-1}\sin\gamma + \left(A_{22}m^2 + k_sA_{44}\cos^2\gamma + A_{66}\sin^2\gamma\right)r^{-2}\right]V \\
&-m\left(A_{22}+k_sA_{44}\right)r^{-2}\cos\gamma W - m\left(B_{12}+B_{66}\right)r^{-1}X' - m\left[B'_{66}r^{-1} + \left(B_{22}+B_{66}\right)r^{-2}\sin\gamma\right]X + B_{66}\Theta'' \\
&+\left(B'_{66} + B_{66}r^{-1}\sin\gamma\right)\Theta' + \left[\left(k_sA_{44}\cos\gamma - B'_{66}\sin\gamma\right)r^{-1} - \left(B_{22}m^2 + B_{66}\sin^2\gamma\right)r^{-2}\right]\Theta = 0, \\
&-\omega^2J_0W - A_{12}r^{-1}\cos\gamma U' - 0.5A_{22}r^{-2}\sin 2\gamma U - m\left(A_{22}+k_sA_{44}\right)r^{-2}\cos\gamma V \\
&+k_sA_{55}W'' + \left(k_sA'_{55} + k_sr^{-1}A_{55}\sin\gamma - \xi\right)W' - \left[\left(A_{22}\cos^2\gamma + k_sA_{44}m^2\right)r^{-2} - 0.5\eta r^{-1}\right]W \\
&+\left(k_sA_{55} - B_{12}r^{-1}\cos\gamma\right)X' + \left(k_sA'_{55} + k_sA_{55}r^{-1}\sin\gamma - 0.5B_{22}r^{-2}\sin 2\gamma\right)X \\
&+m\left(k_sA_{44}r^{-1} - B_{22}r^{-2}\cos\gamma\right)\Theta = 0, \\
&-\omega^2\left(J_1U + J_2X\right) + B_{11}U'' + \left(B'_{11} + B_{11}r^{-1}\sin\gamma\right)U' + \left[B'_{12}r^{-1}\sin\gamma - \left(B_{22}\sin^2\gamma + B_{66}m^2\right)r^{-2}\right]U \\
&+m\left(B_{12}+B_{66}\right)r^{-1}V' + m\left[B'_{12}r^{-1} - \left(B_{22}+B_{66}\right)r^{-2}\sin\gamma\right]V - \left(k_sA_{55} - B_{12}r^{-1}\cos\gamma\right)W' \\
&+\cos\gamma\left(B'_{12}r^{-1} - B_{22}r^{-2}\sin\gamma\right)W + D_{11}X'' + \left(D'_{11} + D_{11}r^{-1}\sin\gamma\right)X' \\
&-\left[k_sA_{55} - D'_{12}r^{-1}\sin\gamma + \left(D_{22}\sin^2\gamma + D_{66}m^2\right)r^{-2}\right]X + m\left(D_{12}+D_{66}\right)r^{-1}\Theta' \\
&+m\left[D'_{12}r^{-1} - \left(D_{22}+D_{66}\right)r^{-2}\sin\gamma\right]\Theta = 0, \\
&-\omega^2\left(J_1V + J_2\Theta\right) - m\left(B_{12}+B_{66}\right)r^{-1}U' - m\left[B'_{66}r^{-1} + \left(B_{22}+B_{66}\right)r^{-2}\sin\gamma\right]U + B_{66}V'' \\
&+\left(B'_{66} + B_{66}r^{-1}\sin\gamma\right)V' + \left[\left(k_sA_{44}\cos\gamma - B'_{66}\sin\gamma\right)r^{-1} - \left(B_{22}m^2 + B_{66}\sin^2\gamma\right)r^{-2}\right]V \\
&+m\left(k_sA_{44}r^{-1} - B_{22}r^{-2}\cos\gamma\right)W - m\left(D_{12}+D_{66}\right)r^{-1}X' - m\left[D'_{66}r^{-1} + \left(D_{22}+D_{66}\right)r^{-2}\sin\gamma\right]X \\
&+D_{66}\Theta'' + \left(D'_{66} + D_{66}r^{-1}\sin\gamma\right)\Theta' - \left[k_sA_{44} + D'_{66}r^{-1}\sin\gamma + \left(D_{22}m^2 + D_{66}\sin^2\gamma\right)r^{-2}\right]\Theta = 0,
\end{aligned} \tag{28}$$

in which prime shows derivate with respect to spatial coordinate x.

Substituting Eqs. (20) and (27) into Eq. (26) brings about the relations below for the boundary conditions:

Clamped (C):

$$U = V = W = 0, \quad X = \Theta = 0.$$

Simply supported (S):

$$
\begin{aligned}
&V = W = 0, \quad \Theta = 0,\\
&A_{11}U' + A_{12}r^{-1}\sin\gamma U + B_{11}X' + B_{12}r^{-1}\sin\gamma X = 0,\\
&B_{11}U' + B_{12}r^{-1}\sin\gamma U + D_{11}X' + D_{12}r^{-1}\sin\gamma X = 0.
\end{aligned}
\tag{29}
$$

Free (F):

$$
\begin{aligned}
&A_{11}U' + A_{12}r^{-1}\sin\gamma U + mA_{12}r^{-1}V + A_{12}r^{-1}\cos\gamma W + B_{11}X' + B_{12}r^{-1}\sin\gamma X + mB_{12}r^{-1}\Theta = 0,\\
&-mA_{66}r^{-1}U + A_{66}V' - A_{66}r^{-1}\sin\gamma V - mB_{66}r^{-1}X + B_{66}\Theta' - B_{66}r^{-1}\sin\gamma\Theta = 0,\\
&W' + X = 0\\
&B_{11}U' + B_{12}r^{-1}\sin\gamma U + mB_{12}r^{-1}V + B_{12}r^{-1}\cos\gamma W + D_{11}X' + D_{12}r^{-1}\sin\gamma X + mD_{12}r^{-1}\Theta = 0,\\
&-mB_{66}r^{-1}U + B_{66}V' - B_{66}r^{-1}\sin\gamma V - mD_{66}r^{-1}X + D_{66}\Theta' - D_{66}r^{-1}\sin\gamma\Theta = 0,
\end{aligned}
$$

5 SOLUTION METHODOLOGY

Due to the mathematical intricacies that appeared in the governing equations (Eq. (28)) and corresponding boundary conditions (Eq. (29)), finding an exact solution is not possible for authors. Thus, a numerical approach is employed in this section of the paper via the DQM. According to the main idea in this method, each derivative of a function like F(x) can be calculated in terms of the values of the function at a pre-selected set of points as [30]

$$\left\{\frac{d^r F}{dx^r}\right\} = \left[X^{(r)}\right]\{F\}, \tag{30}$$

in which, $[X^{rn)}]$ shows the weighting coefficients matrix related to the rth-order derivative and is defined as [30]

$$
X_{ij}^{(1)} = \begin{cases} \dfrac{\prod_{\substack{r=1\\ r\neq i,j}}^{N}(x_i - x_r)}{\prod_{\substack{r=1\\ r\neq j}}^{N}(x_j - x_r)}, & i \neq j \\ \sum_{\substack{r=1\\ r\neq i}}^{N}\dfrac{1}{x_i - x_r}, & i = j \end{cases} \qquad i, j = 1,2,,...,N.
\tag{31}
$$

$$\left[X^{(r)}\right] = \left[X^{(1)}\right]\left[X^{(r-1)}\right], \quad r = 2,3,4,\ldots$$

where N represents the number of points. The minimum number of points to achieve the convergent results depends on the dispersion pattern of the grid points. In the current work, the following set of points ($0 \le x \le L$) is employed which is called the Chebyshev–Gauss–Lobatto dispersion pattern [30]:

$$x_i = 0.5L\left[1 - \cos\left(\frac{i-1}{N-1}\pi\right)\right], \quad i = 1,2,3,\ldots,N \tag{32}$$

Utilizing Eq. (30), the governing equations (Eq. (28)) are presented as

$$[K]\{s\} = \omega^2[M]\{s\}, \tag{33}$$

where $\{s\}$ is displacement vector and $[K]$ and $[M]$ sequentially show the stiffness and mass matrices and are presented in Appendix A.

Employing Eq. (30), the boundary conditions (Eq. (29)) are presented as

$$[H]\{s\} = \{0\}, \tag{34}$$

where $[H]$ is presented in Appendix B.

Simultaneous solutions of Eqs. (33) and (34) lead to inconsistency between the numbers of unknown variables and algebraic equations [29]. To remove it, the grid points can be divided into two groups: the boundary points

(x_1 and x_N) and the domain ones (x_2, x_3 ..., x_{N-2}, x_{N-1}). By neglecting satisfying of Eq. (33) at the boundary points (removing the rows related to the boundary point in each governing equation), the equation below is achieved:

$$\left[\tilde{K}\right]\{s\} = \omega^2\left[\tilde{M}\right]\{s\}, \tag{35}$$

where the sign ~ refers to the corresponding non-square matrices of order (5N-10)×5N. By separating the columns of the matrices related to the domain and boundary points, Eqs. (34) and (35) are represented as follows:

$$\left[\tilde{K}\right]_b\{s\}_b + \left[\tilde{K}\right]_d\{s\}_d = \omega^2\left(\left[\tilde{M}\right]_b\{s\}_b + \left[\tilde{M}\right]_d\{s\}_d\right), \tag{36}$$

$$\left[H\right]_d\{s\}_d + \left[H\right]_b\{s\}_b = \{0\}, \tag{37}$$

where the subscripts "d" and "b" sequentially refer to the domain and boundary points.

Substituting Eq. (37) into Eq. (36) brings about the relation below:

$$\left[K^*\right]\{s\}_d = \omega^2\left[M^*\right]\{s\}_d, \tag{38}$$

where

$$\left[K^*\right] = -\left[\tilde{K}\right]_b\left[H\right]_b^{-1}\left[H\right]_d + \left[\tilde{K}\right]_d, \quad \left[M^*\right] = -\left[\tilde{M}\right]_b\left[H\right]_b^{-1}\left[H\right]_d + \left[\tilde{M}\right]_d. \tag{39}$$

The solution of Eq. (38) provides the eigenvalues of the shell and corresponding eigenvectors. The eigenvalues are complex numbers and for each vibrational mode, the natural frequency (Ω_{mn}) and the corresponding damping ratio (ζ_{mn}) can be calculated in terms of the absolute value (| |), real part (Re), and imaginary part (Im) of the eigenvalue ω_{mn} as [31]

$$\Omega_{mn} = \mathrm{Im}\left(\omega_{mn}\right), \quad \zeta_{mn} = -\frac{\mathrm{Re}\left(\omega_{mn}\right)}{\left|\omega_{mn}\right|}, \tag{40}$$

where the first subscript (m=0,1,2,…) refers to the circumferential wave number and the second one (n=1,2,3,…) refers to the meridional mode number.

The damping ratio is a dimensionless parameter as described in Eq. (40). The dimensionless forms of the aerodynamic pressure (ξ^*) and the natural frequencies are defined accordingly:

$$\xi^* = \frac{10^4\,\xi}{E_m}, \quad \lambda_{nm} = \Omega_{nm}a\sqrt{\frac{\rho_m}{E_m}}. \tag{41}$$

By increasing the aerodynamic pressure generated by the external fluid flow, the damping ratios and natural frequencies are influenced in all vibrational modes. In a special (critical) value of the aerodynamic pressure, the damping ratio of a vibrational mode (flutter mode) declines to negative values (ζ_{mn}<0), which results in aeroelastic instability (flutter phenomenon).

6 NUMERICAL RESULTS

Numerical examples are presented in the current section. The boundary conditions at both ends of the shell are shown utilizing two capital letters which represent the conditions at x=0 and x=L, sequentially. Except for the cases that are described directly, A CC truncated conical shell of a=1 m, L/a=2, γ=30°, and h/a=0.02 is chosen. The main material of the shell epoxy reinforced with GNPs (E_m=2.1 GPa, ν_m=0.34, ρ_m=1150 kg/m^3, E_r=1.01 TPa, ν_r=0.186, ρ_r=1060 kg/m^3, l_r=2.5 µm, w_r=1.5 µm, h_r=1.5 nm) [32-34] of g^*_r=0.01 (1 %) dispersed based on type 4 of n_x=n_z=1.

6.1 Convergence and Verification

For ξ^*=2, the variation of the dimensionless natural frequencies versus the variation of grid points is depicted in Figure 4 for some selected vibrational modes (m=0,1 and n=1,2,…,8). As this figure shows, by growing the number of grid points, convergent results can be achieved. Hereafter, the results are reported using N=15.

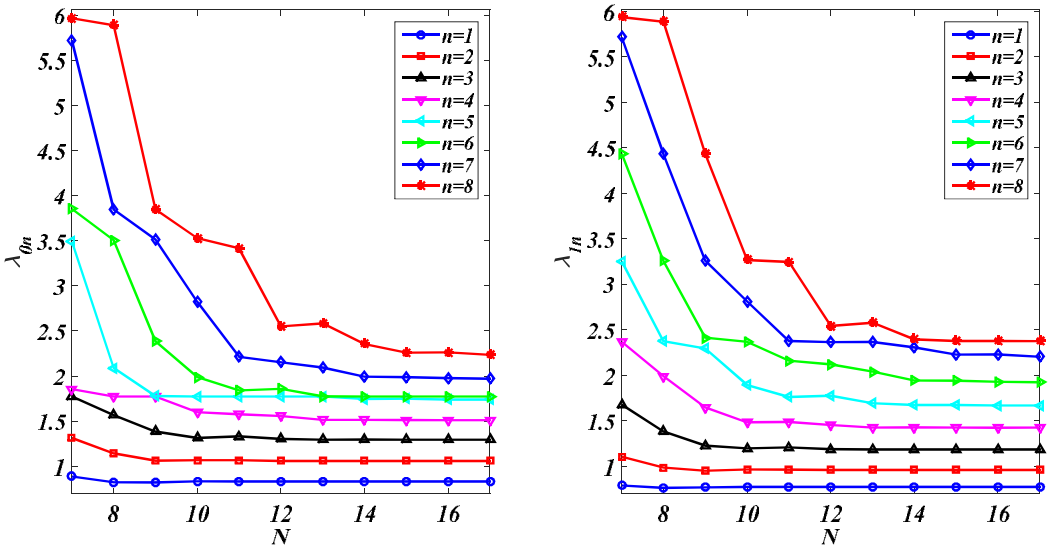

Fig.4
Convergence of the provided solution.

Four examples are presented in this section to confirm the precision of the presented work. As the first one, consider an SC homogenous isotropic conical shell of ν=0.3, γ=45°, h/b=0.01, and $L\sin\gamma/b$=0.5. By neglecting the effect of aerodynamic pressure (ξ^*=0), the dimensionless natural frequencies ($\lambda^*_{nm}=\Omega_{nm}b\sqrt{\rho_m\left(1-\nu_m^2\right)/E_m}$) are presented in Table 1 for m=0,1,…,9 and n=1 alongside those reported by Liew et al. [35]. As observed, the maximum discrepancy is 0.14 % which shows a good agreement between the present results predicted based on the FSDT and those predicted by Liew et al. [35] based on Love's shell theory. It should be noticed that for thin shells, there are good agreements between the results obtained based on the FSDT and those obtained based on a classical shell theory. But as the thickness of the shell grows, classical shell theories lose their accuracy, and discrepancies between the results obtained based on them and those obtained based on the FSDT increase.
As the second example, consider a CF conical shell of a=3.35 in, b=5.58 in, $L\cos\gamma$=12 in, h=0.01 in, made of Type 304 stainless steel (E=193 GPa, ν=0.29, ρ=8000 kg/m^3) with no external fluid flow (ξ^*=0). For n=1, the variations of the natural frequencies versus the variations of the circumferential wave number (m=3,4,…,11) are depicted in Figure 5 alongside the experimental ones presented by Platus [36]. As this figure shows, there is an acceptable agreement between the numerical results predicted in the present work and the experimental ones presented in Ref. [36] which confirms the accuracy of the presented work.

Table 1
The dimensionless natural frequencies of a homogenous isotropic conical shell.

m	0	1	2	3	4	5	6	7	8	9
Present	0.8694	0.8115	0.6611	0.5246	0.4318	0.3825	0.3734	0.3980	0.4468	0.5117
Liew et al. [35]	0.8691	0.8113	0.6610	0.5244	0.4316	0.3822	0.3732	0.3980	0.4472	0.5124
Discrepancy (%)	0.03	0.02	0.02	0.04	0.05	0.08	0.05	0.00	0.09	0.14

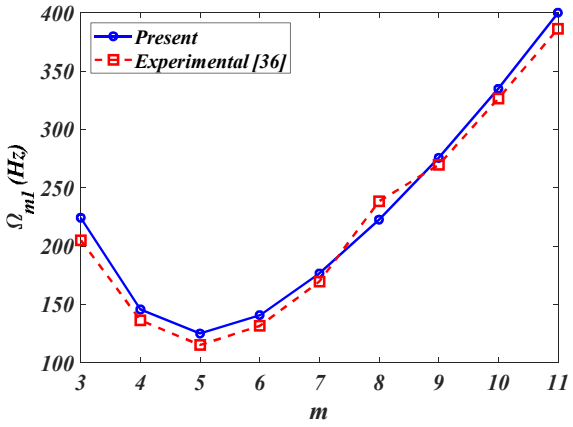

Fig.5
The variations of the natural frequencies of a CF conical shell versus the variations of the circumferential wave number.

Table 2
The natural frequencies (kHz) of a one-directional FG GNP-enriched conical shell.

m	n	UD		FG-V		FG-A	
		Present	Afshari [37]	Present	Afshari [37]	Present	Afshari [37]
1	1	0.3105	0.3105	0.3105	0.3105	0.3099	0.3099
	2	0.3892	0.3892	0.3871	0.3871	0.3886	0.3886
	3	0.4971	0.4971	0.4927	0.4927	0.4950	0.4950
	4	0.5657	0.5657	0.5536	0.5536	0.5566	0.5565
2	1	0.1807	0.1807	0.1780	0.1781	0.1794	0.1794
	2	0.3694	0.3694	0.3638	0.3639	0.3664	0.3663
	3	0.4975	0.4975	0.4836	0.4837	0.4869	0.4868
	4	0.6248	0.6248	0.5996	0.5997	0.6037	0.6035
3	1	0.1518	0.1518	0.1428	0.1432	0.1451	0.1447
	2	0.3137	0.3137	0.3013	0.3017	0.3049	0.3045
	3	0.4589	0.4589	0.4384	0.4387	0.4428	0.4424
	4	0.6082	0.6082	0.5739	0.5743	0.5793	0.5788
4	1	0.1901	0.1901	0.1727	0.1735	0.1763	0.1755
	2	0.3264	0.3264	0.3023	0.3032	0.3076	0.3066
	3	0.4699	0.4699	0.4370	0.4379	0.4433	0.4423
	4	0.6285	0.6285	0.5822	0.5831	0.5895	0.5885

As the third example, consider a CS truncated conical shell (a=0.5 m, L/a=4, γ=20°, h/a=0.1) made of epoxy (ν_m=0.34, E_m=3 GPa, ρ_m=1200 kg/m^3) enriched with GNPs (ν_r=0.186, E_r=1.01 TPa, ρ_r=1060 kg/m^3, l_r=1 μm, w_r=0.5 μm, h_r=0.5 nm) of g^*_r=0.01 dispersed along the thickness direction. Several one-directional dispersion patterns of GNPs through the thickness direction are selected including uniform dispersion (UD) pattern (type 1, n_x=n_z=0), FG-V pattern (type 1, n_x=0, n_z=1), and FG-A pattern (type 2, n_x=0, n_z=1). By neglecting the effect of aerodynamic pressure (ξ^*=0), the natural frequencies in the first to fourth vibrational modes (n=1,2,3,4) are reported in Table 2 for m=1,2,3,4 along with those predicted by Afshari [37]. Also, the corresponding vibrational mode shapes are provided in Figure 6 for UD. As shown in Table 2, the results of the presented work agree with those reported by Afshari in Ref. [37] which proves the precision of the current work.

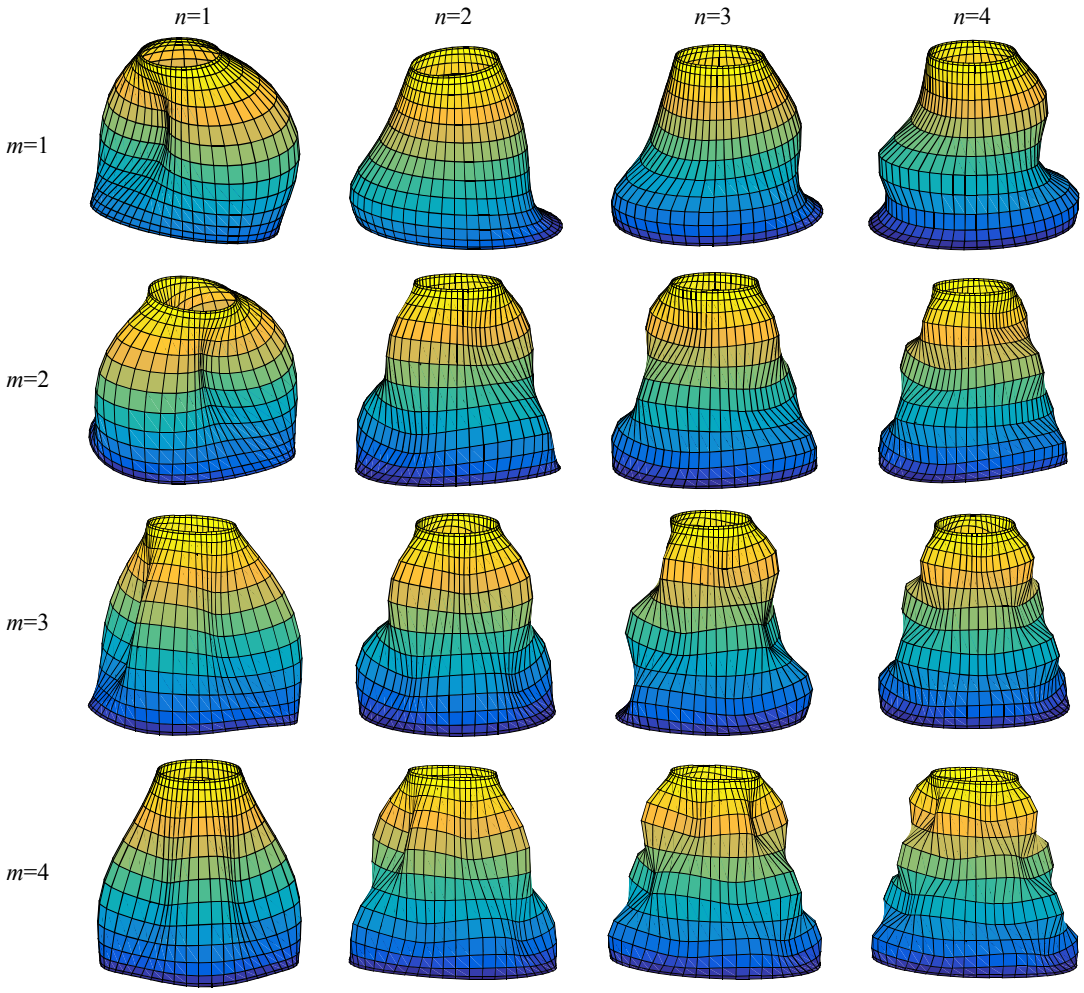

Fig.6
Vibrational mode shapes of a CS truncated conical shell for some selected vibrational modes.

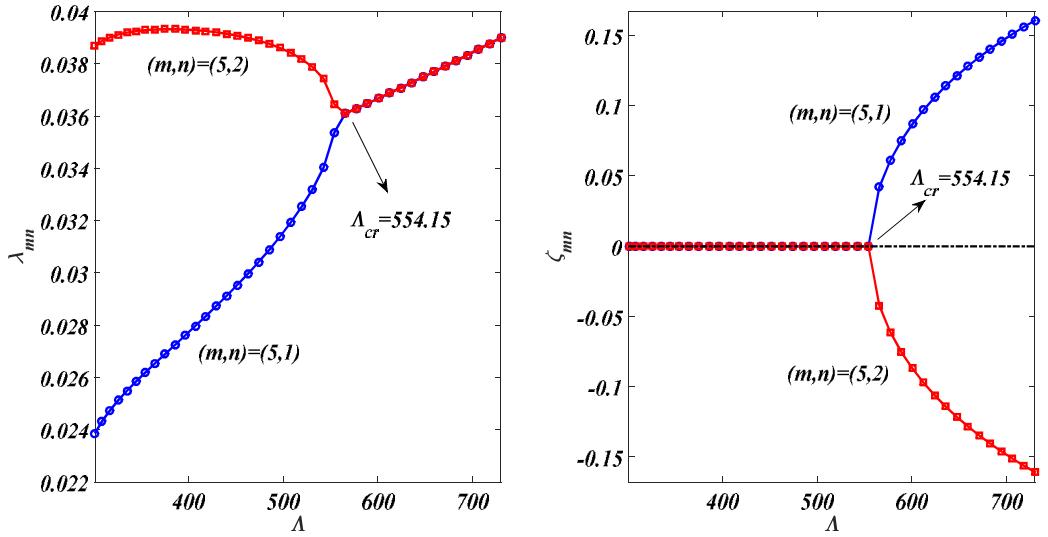

Fig.7
Flutter boundaries for an SS homogenous isotropic conical shell.

Table 3
The critical aerodynamic pressure for an SS homogenous isotropic conical shell.

	Present	Mahmoudkhani et al. [14]	Rahmanian and Javadi [15]	Nasution et al. [17]
Λ_{cr}	554.15	570	566.4	548.89

As the fourth example, consider a simply supported (SS) homogenous isotropic conical shell of ν=0.29, E=44.8175 GPa, ρ=8900 kg/m^3, α=5°, a=191.719 mm, h=1.2954 mm, and L=1.5586 m. Figure 7 shows the variation of the natural frequencies and corresponding damping ratios versus the variation of the aerodynamic pressure ($\Lambda = 12\left(1-\nu^2\right)\rho_\infty U_s^2 a^3 M_\infty^2 \big/ Eh^3\sqrt{M_\infty^2-1}$) in dimensionless forms for For m=5 and n=1,2. As this figure shows, in a special (critical) value of the dimensionless aerodynamic pressure (Λ_{cr}=554.15), the natural frequencies of modes (m,n)=(5,1) and (m,n)=(5,2) coalesce and the damping ratio of the mode (5,2) becomes a negative value which results in unstable oscillation called flutter. The critical values of the aerodynamic pressure in dimensionless form (Λ_{cr}) presented in other works are presented in Table 3. As discovered, good agreements exist between the present results and those reported in Refs. [14, 15, 17].

6.2 Parametric Study

A parametric investigation is presented in the current section to discover the impacts of several parameters on the flutter boundaries including mass fraction and dispersion pattern of the GNPs, gradient indices, boundary conditions, and the semi-vertex angle. As Figure 7 shows, the predictions of the critical aerodynamic pressure utilizing the damping ratios and the natural frequencies result in the same results. Thus, in what follows, the critical aerodynamic pressure is determined utilizing the variation of the natural frequencies versus the variations of the aerodynamic pressure. As it is impossible to guess the flutter mode between the vibrational modes, in this paper, the variations of the natural frequencies versus the variations of the aerodynamic pressure are explored for m=0,1,2,…,5 and n=1,2,3,…,8, and the flutter mode is determined between these 48 vibrational modes. It is noteworthy that the variation of all these vibrational modes versus the variations of the aerodynamic pressure is not depicted in what follows and only two coalesced vibrational modes associated with the flutter are illustrated.

By neglecting the effect of aerodynamic pressure (ξ^*=0), Figure 8 shows the variation of the first eight natural frequencies (n=1,2,..,8) in dimensionless forms versus the variation of the circumferential wave number (m=1,2,…,20). This figure reveals that by growing the circumferential wave number, the natural frequencies for n=1,2,..,5 experience an initial reduction followed by an increase, and the natural frequencies for n=6,7,8 experience an initial growth and a secondary reduction followed by an increase.

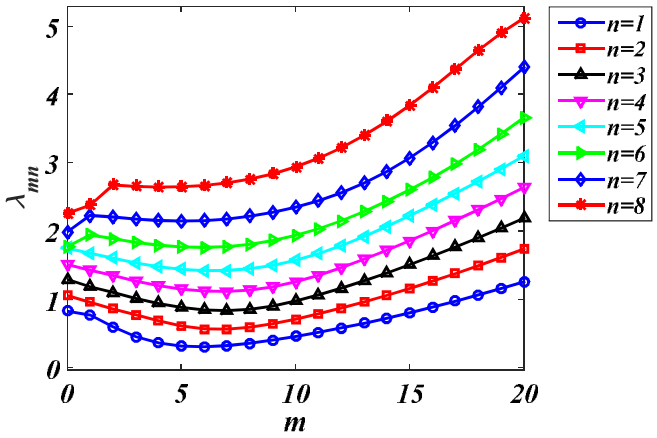

Fig.8
The relevance of the natural frequencies on the circumferential wave number.

The impact of the mass fraction of GNPs on the critical aerodynamic pressure is studied in Figure 9. Due to the high value of the elastic modulus of the GNPs rather than the polymeric matrix, subjoining the GNPs to the matrix enhances the stiffness of the shell and brings about higher aeroelastic stability. This figure reveals that the mass fraction of GNPs has no impact on the flutter mode and by growing its value from 0.25 % to 1 %, the critical aerodynamic pressure experiences more than 141 % enhancement.

The flutter boundaries of a two-directional FG GNP-enriched truncated conical shell for the various types of dispersion patterns of the GNPs are investigated in Figure 10. This figure reveals that the lowest critical aerodynamic pressure belongs to type 1 and the highest aeroelastic stability can be achieved when the GNPs are dispersed based on type 4. Thus, according to Figure 2, it can be claimed that to achieve higher aeroelastic stability in the GNP-enriched truncated conical shells, it is more useful to disperse the GNPs near the small radius (x=0) and the inner surface of the shell (z=-0.5h). To show the high importance of the dispersion pattern on the GNPs, it can be concluded from Figure 10 that the critical aerodynamic pressure for type 4 is about 182 % higher than for type 1. Figure 10 also shows that the flutter mode might be influenced by the dispersion pattern of GNPs along the meridional direction.

The relevance of the flutter boundaries on the power-law index n_x is explored in Figure 11. As observed, the aeroelastic stability improves by growing the value of the power-law index n_x. In conjunction with Figure 3, it can be claimed that to enhance the aeroelastic stability, it is more helpful to use a smoother variation in the variation of the mass fraction of the GNPs in the meridional direction.

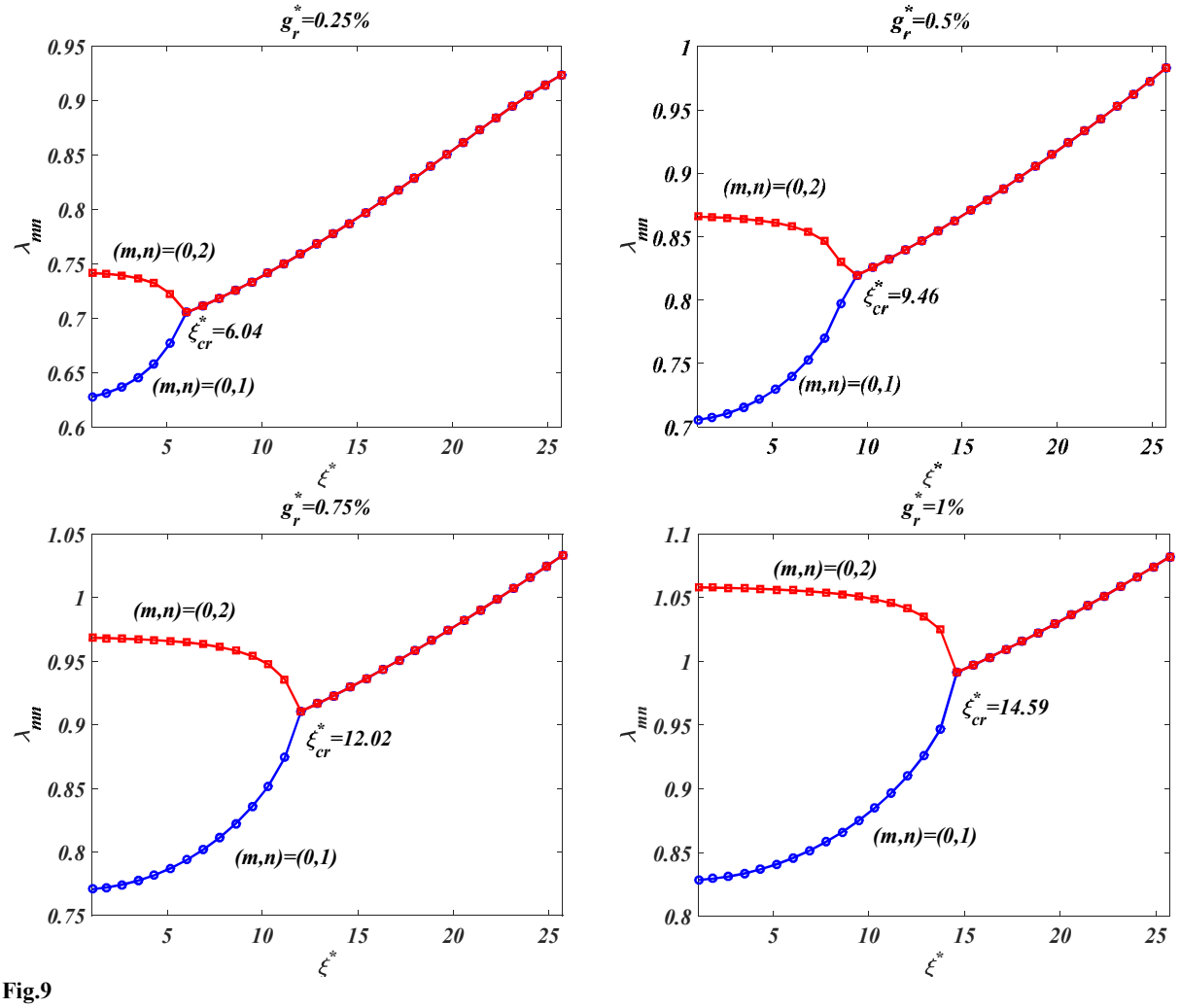

Fig.9
The effects of the mass fraction of GNPs on the flutter boundaries.

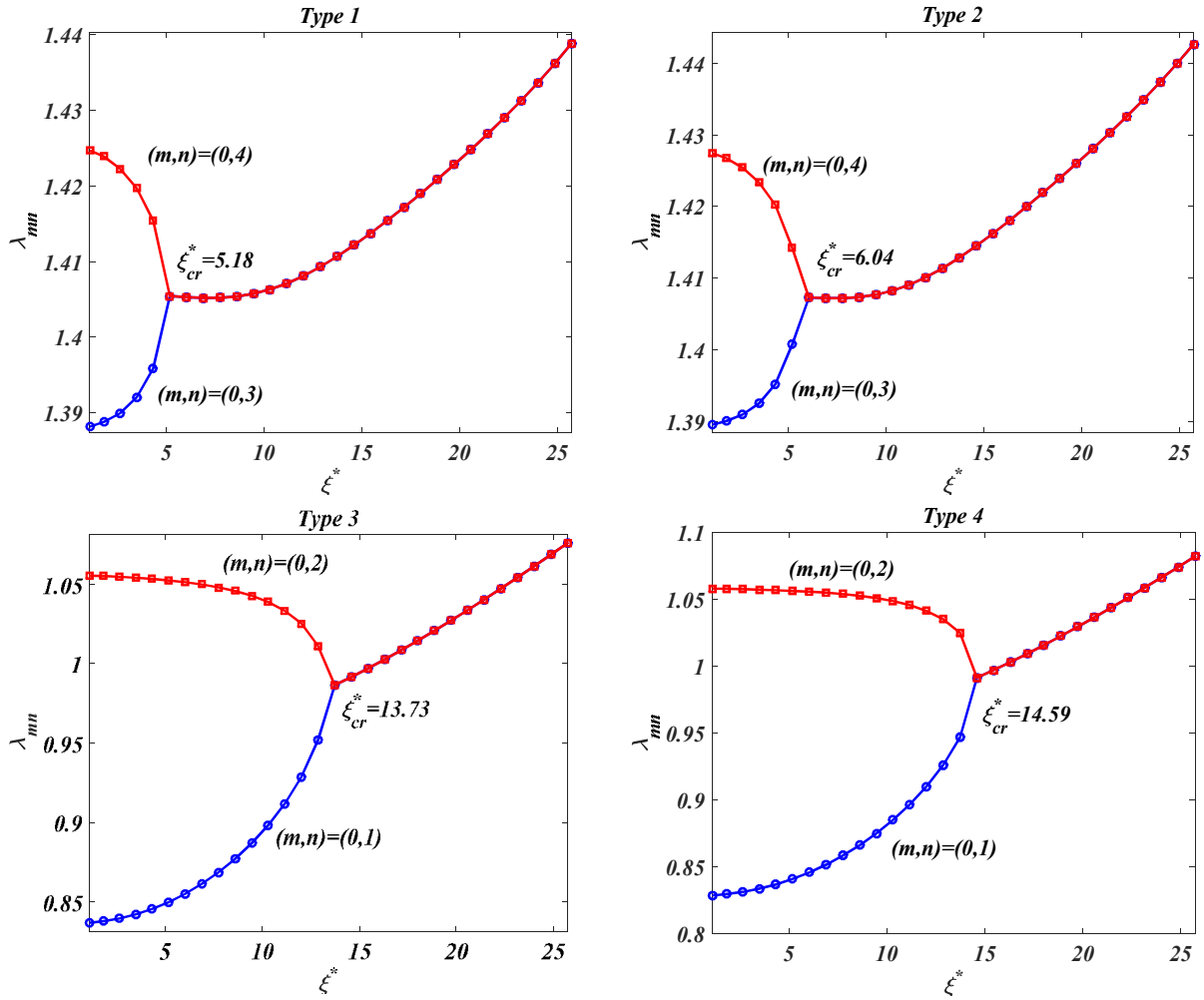

Fig.10
The effects of the dispersion pattern of GNPs on the flutter boundaries.

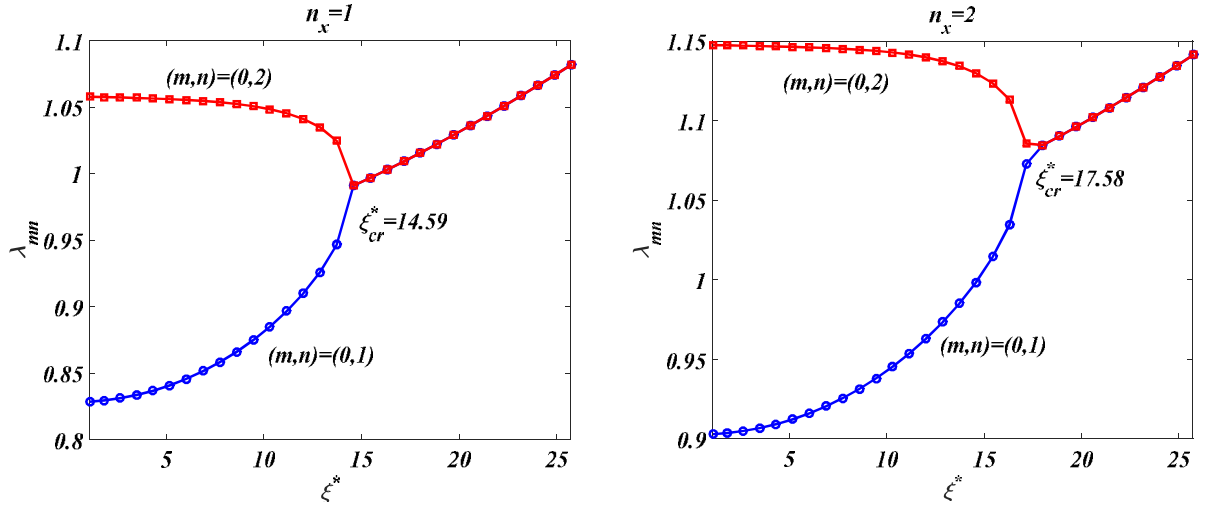

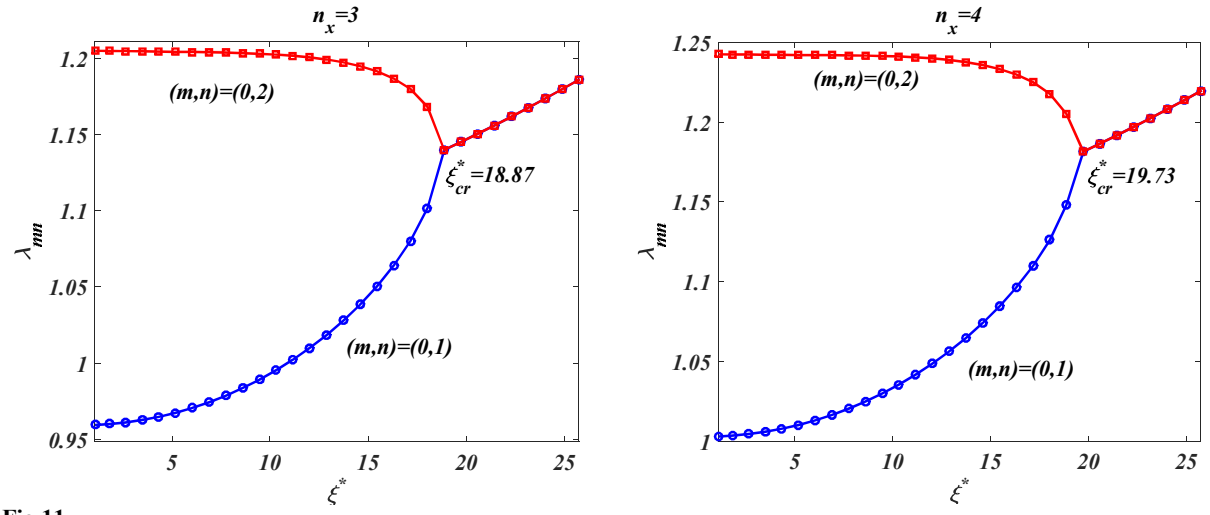

Fig.11
The effects of the power-law index n_x on the flutter boundaries.

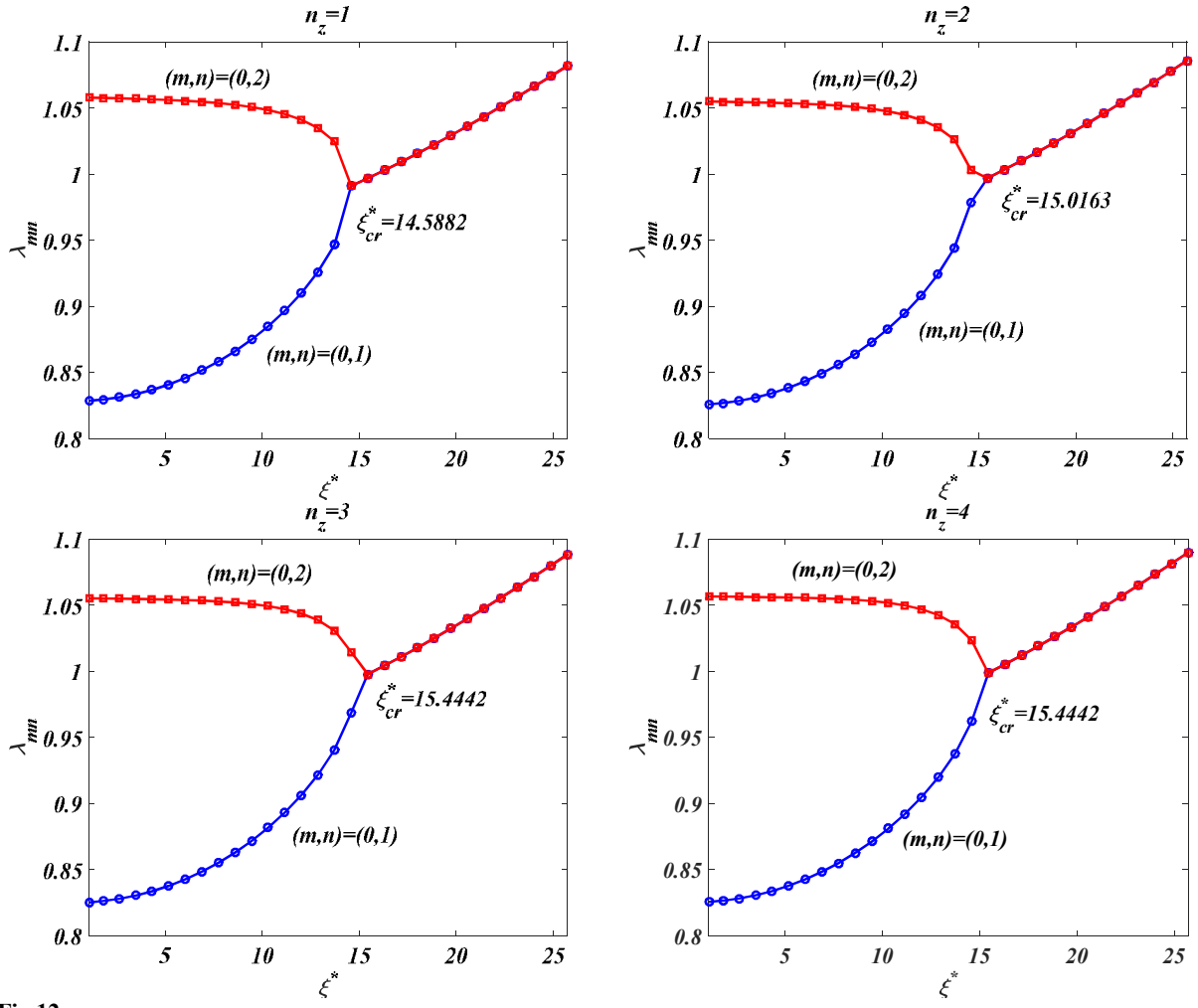

Fig.12
The impacts of the power-law index n_z on the flutter boundaries.

The relevance of the aeroelastic stability on the power-law index n_z is explored in Figure 12. As shown in this figure, the aeroelastic stability experiences a small growth by growing the power-law index n_z. In conjunction with Figure 3, it can be claimed that to reach higher aeroelastic stability, it is more beneficial to disperse the GNPs near the inner surface of the shell.

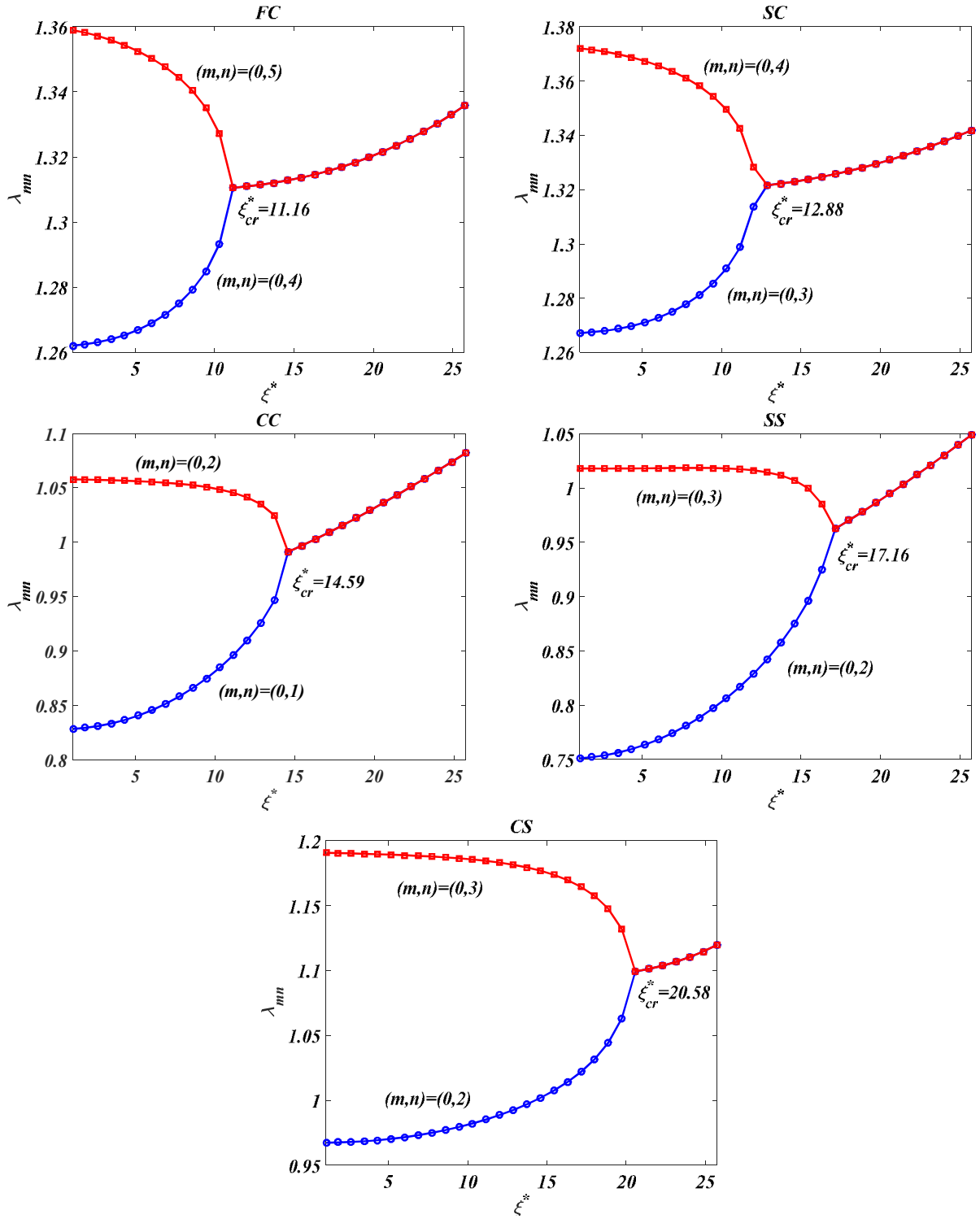

Fig.13
The effects of boundary conditions on the flutter boundaries.

Figures 11 and 12 show that the power-law indices n_x and n_z do not affect the flutter mode. It can be concluded that growth in the power-law index n_x from 1 to 4 brings about a more than 35 % increase in the critical aerodynamic pressure and growing the power-law index n_z from 1 to 4 leads to less than 6 % growth in the critical aerodynamic pressure. In other words, the variation of the mass fraction of the GNPs along the meridional direction has a stronger impact on the flutter boundaries in comparison with the variation of the mass fraction of the GNPs along the thickness direction.

Figure 13 is provided to check the relevance of the flutter boundaries on the boundary conditions at both ends of the shell. It is shown by other authors that the more constrained condition at the edges of the shell brings about higher natural frequencies and the condition at the large radius of the shell ($x=L$) has a more remarkable impact on the natural frequencies than the condition at the small radius of the shell ($x=0$) [38]. In other words, it is shown by other authors that the highest natural frequencies belong to the CC shell. Figure 13 shows that the flutter mode is dependent on the boundary conditions and for this case study, the highest aerodynamic pressure belongs to the CS shell. Figure 13 reveals that the highest aeroelastic stability does not necessarily belong to the CC shell and the more restricted condition at the edges of the shell may not result in the higher aerodynamic pressure.

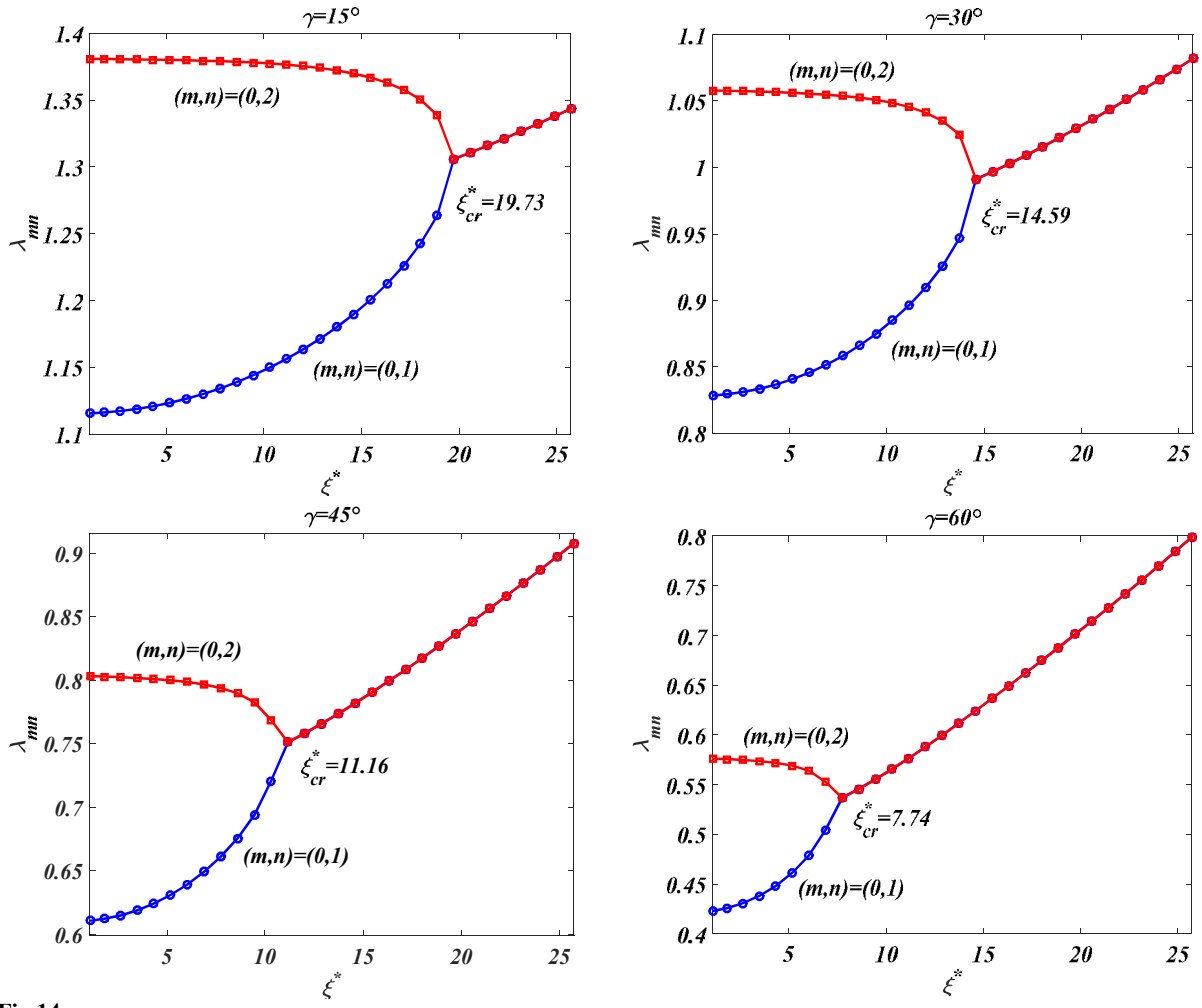

Fig.14
The influences of the semi-vertex angle on the flutter boundaries.

The effect of the semi-vertex angle on the aeroelastic stability is investigated in Figure 14. By considering specific values for the small radius and the length of the shell, an increase in the semi-vertex angle increases the radius of the shell which leads to a growth in the inertia and a decrease in the stiffness of the shell [39]. Thus, as Figure 14 shows, the critical aerodynamic pressure of the shell experiences a reduction by growing the semi-vertex angle. As this figure shows, the flutter mode is not influenced by the semi-vertex angle, and by increasing the semi-vertex angle from 15° to 60°, the critical aerodynamic pressure experiences about 62 % reduction. In other words, a cylindrical (γ=0) shell of radius $r=a$ is more stable against the supersonic fluid flows than a truncated conical shell of small radius $r=a$. Thus, if it is necessary to use a truncated conical shell (for example to affect thermodynamic characteristics), the smaller semi-vertex angles should be preferred.

The effects of the thickness-to-small radius ratio on the flutter boundaries are investigated in Figure 15. This figure shows that an increase in the thickness of the shell brings about a higher rigidity and improves the aeroelastic stability of the shell. By increasing the thickness-to-small radius ratio from 0.015 to 0.0225, the critical aerodynamic pressure experiences about 120 % enhancement. Although it is a significant improvement, the mass of the shell grows by increasing the thickness which is not a desired item in aerospace structures.

The influences of the length-to-small radius ratio on the flutter boundaries are studied in Figure 16. As observed in this figure, the aeroelastic stability dramatically decreases by increasing the length of the shell. The reason behind this is the reduction in the flexural rigidity of the shell created by the increase in the length. As observed, by increasing the length-to-small radius ratio from 1.5 to 2.25, the critical aerodynamic pressure experiences about 41 % reduction.

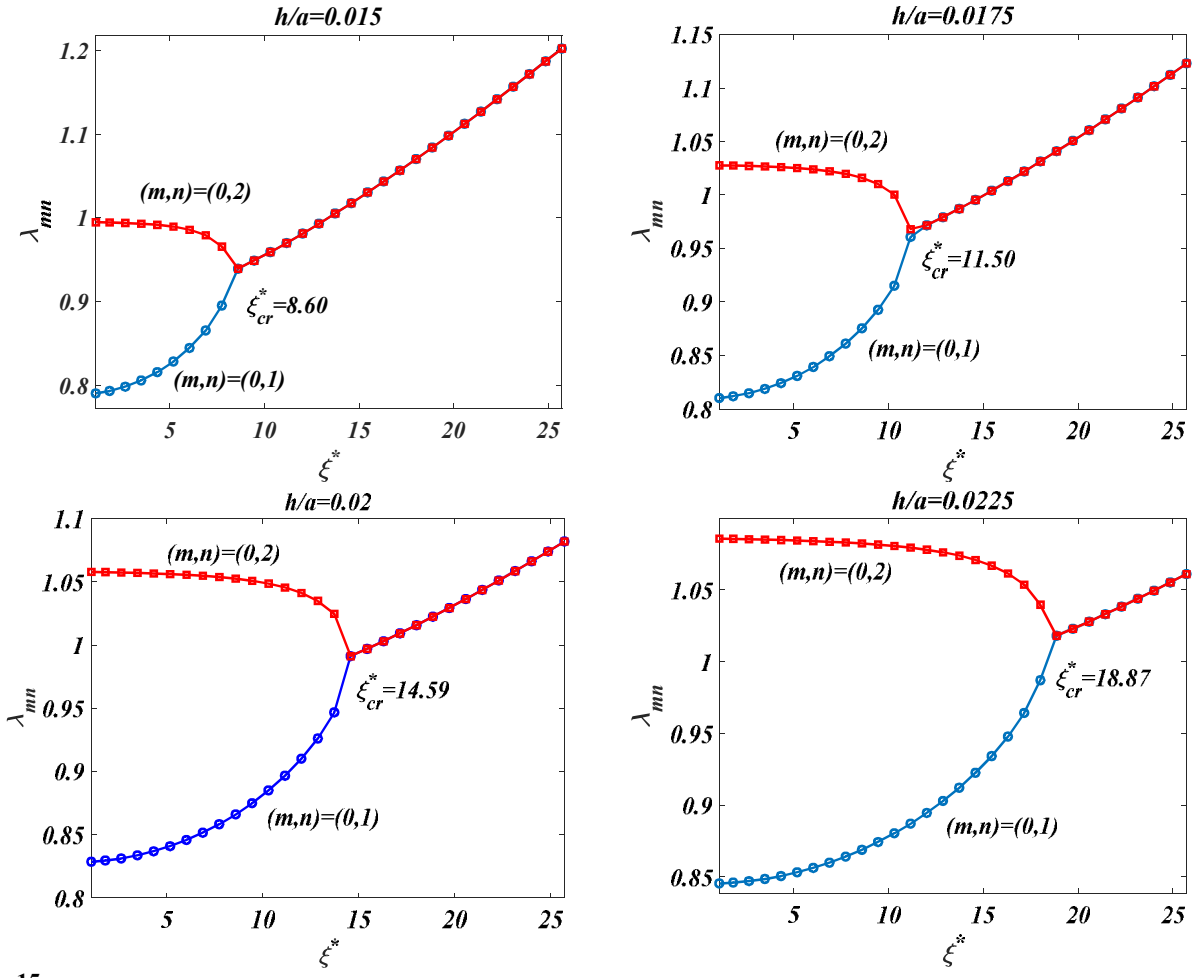

Fig.15
The impacts of the thickness-to-small radius ratio on the flutter boundaries.

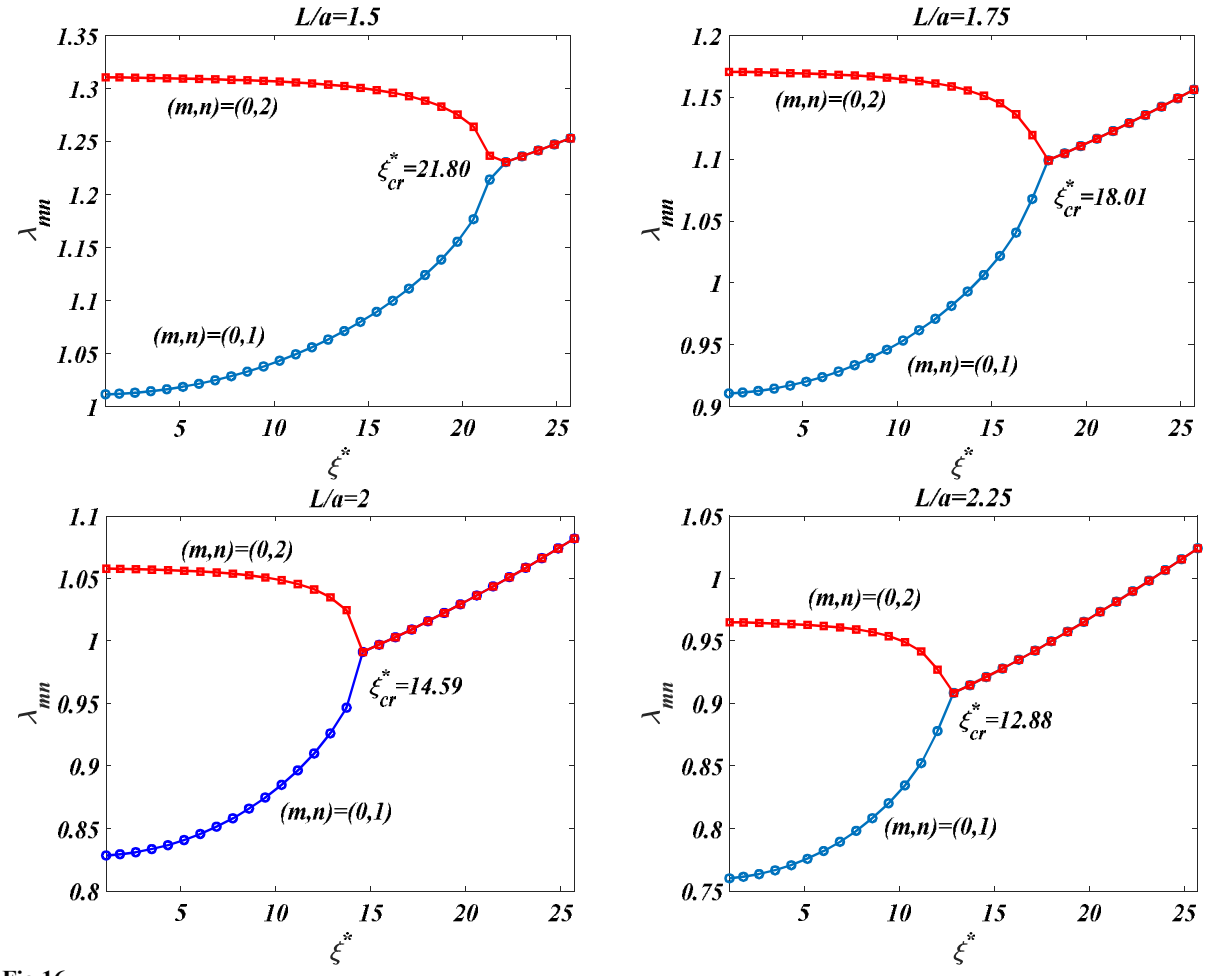

Fig.16
The impacts of the length-to-small radius ratio on the flutter boundaries.

7 CONCLUSIONS

The supersonic flutter analysis of a two-directional FG GNP-enriched truncated conical shell was studied in the current work. Modeling of the shell was performed using the FSDT and modeling of the aerodynamic pressure created by the external fluid flow was performed utilizing piston theory. The main findings of the paper are listed in the statements below:

Subjoining the GNPs to the polymeric matrix expands the flutter boundaries of the shell.

To achieve higher aeroelastic stability in the GNP-enriched truncated conical shells, it is more beneficial to disperse the GNPs near the small radius and inner surface of the shell.

The variation of the mass fraction of the GNPs along the meridional direction has a stronger impact on the flutter boundaries in comparison with the variation of the mass fraction of the GNPs in the thickness direction.

The more restricted conditions at the edges of the shell (utilizing clamped edges rather than simply supported ones and simply supported edges rather than free ones) bring about higher natural frequencies but they do not necessarily result in higher aeroelastic stability.

To achieve higher aeroelastic stability of a conical shell, the smaller values of the semi-vertex angle and length, and higher value of the thickness should be utilized.

APPENDIX A

$$\{s\}_{5N\times 1}=\begin{Bmatrix}\{U\}\\ \{V\}\\ \{W\}\\ \{X\}\\ \{\Theta\}\end{Bmatrix},\quad [K]=\begin{bmatrix}[k_{11}] & \dots & [k_{15}]\\ \vdots & \ddots & \vdots\\ [k_{51}] & \dots & [k_{55}]\end{bmatrix},\quad [M]=\begin{bmatrix}[I_0] & [0] & [0] & [I_1] & [0]\\ [0] & [I_0] & [0] & [0] & [I_1]\\ [0] & [0] & [I_0] & [0] & [0]\\ [I_1] & [0] & [0] & [I_2] & [0]\\ [0] & [I_1] & [0] & [0] & [I_2]\end{bmatrix}, \tag{A-1}$$

where $[0]_{N\times N}$ and $I_{N\times N}$ respectively stand for zero and the identity matrices and $[I_0]$, $[I_1]$, and $[I_2]$ are the following diagonal matrices:

$$\left[I_j\right]_{ii}=J_j\big|_{x=x_i}. \tag{A-2}$$

Also, $[k_{11}]$-$[k_{55}]$ are defined as

$$\begin{aligned}
[k_{11}]&=[a_{11}]\left[X^{(2)}\right]+\left([da_{11}]+\sin\gamma[a_{11}][R_1]\right)\left[X^{(1)}\right]+\sin\gamma[da_{12}][R_1]-\left(\sin^2\gamma[a_{22}]+m^2[a_{66}]\right)[R_2],\\
[k_{12}]&=m\left\{\left([a_{12}]+[a_{66}]\right)[R_1]\left[X^{(1)}\right]+[da_{12}][R_1]-\sin\gamma\left([a_{22}]+[a_{66}]\right)[R_2]\right\},\\
[k_{13}]&=\cos\gamma[a_{12}][R_1]\left[X^{(1)}\right]+\cos\gamma[da_{12}][R_1]-0.5\sin 2\gamma[a_{22}][R_2],\\
[k_{14}]&=[b_{11}]\left[X^{(2)}\right]+\left([db_{11}]+\sin\gamma[b_{11}][R_1]\right)\left[X^{(1)}\right]+\sin\gamma[db_{12}][R_1]-\left(\sin^2\gamma[b_{22}]+m^2[b_{66}]\right)[R_2],\\
[k_{15}]&=m\left\{\left([b_{12}]+[b_{66}]\right)[R_1]\left[X^{(1)}\right]+[db_{12}][R_1]-\sin\gamma\left([b_{22}]+[b_{66}]\right)[R_2]\right\},\\
[k_{21}]&=-m\left\{\left([a_{12}]+[a_{66}]\right)[R_1]\left[X^{(1)}\right]+[da_{66}][R_1]+\sin\gamma\left([a_{22}]+[a_{66}]\right)[R_2]\right\},\\
[k_{22}]&=[a_{66}]\left[X^{(2)}\right]+\left([da_{66}]+\sin\gamma[a_{66}][R_1]\right)\left[X^{(1)}\right]-\sin\gamma[da_{66}][R_1]\\
&\quad-\left(m^2[a_{22}]+k_s\cos^2\gamma[a_{44}]+\sin^2\gamma[a_{66}]\right)[R_2],\\
[k_{23}]&=-m\cos\gamma\left([a_{22}]+k_s[a_{44}]\right)[R_2],\\
[k_{24}]&=-m\left\{\left([b_{12}]+[b_{66}]\right)[R_1]\left[X^{(1)}\right]+[db_{66}][R_1]+\sin\gamma\left([b_{22}]+[b_{66}]\right)[R_2]\right\},\\
[k_{25}]&=[b_{66}]\left[X^{(2)}\right]+\left([db_{66}]+\sin\gamma[b_{66}][R_1]\right)\left[X^{(1)}\right]+\left(k_s\cos\gamma[a_{44}]-\sin\gamma[db_{66}]\right)[R_1]\\
&\quad-\left(m^2[b_{22}]+\sin^2\gamma[b_{66}]\right)[R_2],\\
[k_{31}]&=-\cos\gamma[a_{12}][R_1]\left[X^{(1)}\right]-0.5\sin 2\gamma[a_{22}][R_2],\\
[k_{32}]&=-m\cos\gamma\left([a_{22}]+k_s[a_{44}]\right)[R_2],\\
[k_{33}]&=k_s[a_{55}]\left[X^{(2)}\right]+\left(k_s[da_{55}]+k_s\sin\gamma[a_{55}][R_1]-\xi I\right)\left[X^{(1)}\right]\\
&\quad-\left(\cos^2\gamma[a_{22}]+k_sm^2[a_{44}]\right)[R_2]+0.5\eta[R_1],\\
[k_{34}]&=\left(k_s[a_{55}]-\cos\gamma[b_{12}][R_1]\right)\left[X^{(1)}\right]+k_s[da_{55}]+k_s\sin\gamma[a_{55}][R_1]-0.5\sin 2\gamma[b_{22}][R_2],\\
[k_{35}]&=m\left(k_s[a_{44}][R_1]-\cos\gamma[b_{22}][R_2]\right),\\
[k_{41}]&=[b_{11}]\left[X^{(2)}\right]+\left([db_{11}]+\sin\gamma[b_{11}][R_1]\right)\left[X^{(1)}\right]+\sin\gamma[db_{12}][R_1]-\left(\sin^2\gamma[b_{22}]+m^2[b_{66}]\right)[R_2],\\
[k_{42}]&=m\left\{\left([b_{12}]+[b_{66}]\right)[R_1]\left[X^{(1)}\right]+[db_{12}][R_1]-\sin\gamma\left([b_{22}]+[b_{66}]\right)[R_2]\right\},\\
[k_{43}]&=-\left(k_s[a_{55}]-\cos\gamma[b_{12}][R_1]\right)\left[X^{(1)}\right]+\cos\gamma[db_{12}][R_1]-0.5\sin 2\gamma[b_{22}][R_2],\\
[k_{44}]&=[d_{11}]\left[X^{(2)}\right]+\left([dd_{11}]+\sin\gamma[d_{11}][R_1]\right)\left[X^{(1)}\right]-k_s[a_{55}]+\sin\gamma[dd_{12}][R_1]\\
&\quad-\left(\sin^2\gamma[d_{22}]+m^2[d_{66}]\right)[R_2],
\end{aligned} \tag{A-3}$$

$$[k_{45}]=m\left\{\left([d_{12}]+[d_{66}]\right)[R_1]\left[X^{(1)}\right]+[dd_{12}][R_1]-\sin\gamma\left([d_{22}]+[d_{66}]\right)[R_2]\right\},$$
$$[k_{51}]=-m\left\{\left([b_{12}]+[b_{66}]\right)[R_1]\left[X^{(1)}\right]+[db_{66}][R_1]+\sin\gamma\left([b_{22}]+[b_{66}]\right)[R_2]\right\},$$
$$[k_{52}]=[b_{66}]\left[X^{(2)}\right]+\left([db_{66}]+\sin\gamma[b_{66}][R_1]\right)\left[X^{(1)}\right]+\left(k_s\cos\gamma[a_{44}]-\sin\gamma[db_{66}]\right)[R_1]$$
$$-\left(m^2[b_{22}]+\sin^2\gamma[b_{66}]\right)[R_2],$$
$$[k_{53}]=m\left\{k_s[a_{44}][R_1]-\cos\gamma[b_{22}][R_2]\right\},$$
$$[k_{54}]=-m\left\{\left([d_{12}]+[d_{66}]\right)[R_1]\left[X^{(1)}\right]+[dd_{66}][R_1]+\sin\gamma\left([d_{22}]+[d_{66}]\right)[R_2]\right\},$$
$$[k_{55}]=[d_{66}]\left[X^{(2)}\right]+\left([dd_{66}]+\sin\gamma[d_{66}][R_1]\right)\left[X^{(1)}\right]-k_s[a_{44}]-\sin\gamma[dd_{66}][R_1]$$
$$-\left(m^2[d_{22}]+\sin^2\gamma[d_{66}]\right)[R_2],$$

where some diagonal matrices are defined as

$$[R_1]_{ii}=\left.\frac{1}{r}\right|_{x=x_i},\qquad [R_2]_{ii}=\left.\frac{1}{r^2}\right|_{x=x_i},\qquad [a_{pq}]_{ii}=\left.A_{pq}\right|_{x=x_i},\qquad [b_{pq}]_{ii}=\left.B_{pq}\right|_{x=x_i},$$
$$[d_{pq}]_{ii}=\left.D_{pq}\right|_{x=x_i},\quad [da_{pq}]_{ii}=\left.A'_{pq}\right|_{x=x_i},\quad [db_{pq}]_{ii}=\left.B'_{pq}\right|_{x=x_i},\quad [dd_{pq}]_{ii}=\left.D'_{pq}\right|_{x=x_i}. \tag{A-4}$$

APPENDIX B

$$[H]_{10\times 5N}=\begin{bmatrix}\{H_{11}\} & \{H_{12}\} & \{H_{13}\} & \{H_{14}\} & \{H_{15}\}\\ \vdots & \vdots & \vdots & \vdots & \vdots\\ \{H_{101}\} & \{H_{102}\} & \{H_{103}\} & \{H_{104}\} & \{H_{105}\}\end{bmatrix}, \tag{B-1}$$

where $\{H_{11}\}-\{H_{55}\}$ are related to the condition at x=0 and are presented in the relations below:

Clamped(C):

$$\{H_{ij}\}=\begin{cases}\{I_1\} & i=j\\ \{0\}_{1\times N} & i\neq j\end{cases}\quad i,j=1,2,\ldots,5.$$

Simply supported(S):

$$\{H_{ij}\}=\begin{cases}A_{11}^0\{X_1^{(1)}\}+A_{12}^0a^{-1}\sin\gamma\{I_1\} & ij=11\\ B_{11}^0\{X_1^{(1)}\}+B_{12}^0a^{-1}\sin\gamma\{I_1\} & ij=14,41\\ D_{11}^0\{X_1^{(1)}\}+D_{12}^0a^{-1}\sin\gamma\{I_1\} & ij=44\\ \{I_1\} & ij=22,33,55\\ \{0\}_{1\times N} & \text{else}\end{cases}\quad i,j=1,2,\ldots,5. \tag{B-2}$$

$\text{Free}(\text{F})$:

$$\{H_{11}\}=A_{11}^{0}\left\{X_{1}^{(1)}\right\}+A_{12}^{0}a^{-1}\sin\gamma\{I_1\},\quad \{H_{12}\}=mA_{12}^{0}a^{-1}\{I_1\},\quad \{H_{13}\}=A_{12}^{0}a^{-1}\cos\gamma\{I_1\},$$

$$\{H_{14}\}=B_{11}^{0}\left\{X_{1}^{(1)}\right\}+B_{12}^{0}a^{-1}\sin\gamma\{I_1\},\quad \{H_{15}\}=mB_{12}^{0}a^{-1}\{I_1\},\quad \{H_{21}\}=-mA_{66}^{0}a^{-1}\{I_1\},$$

$$\{H_{22}\}=A_{66}^{0}\left\{X_{1}^{(1)}\right\}-A_{66}^{0}a^{-1}\sin\gamma\{I_1\},\quad \{H_{23}\}=\{0\}_{1\times N},\quad \{H_{24}\}=-mB_{66}^{0}a^{-1}\{I_1\},$$

$$\{H_{25}\}=B_{66}^{0}\left\{X_{1}^{(1)}\right\}-B_{66}^{0}a^{-1}\sin\gamma\{I_1\},\quad \{H_{31}\}=\{H_{32}\}=\{H_{35}\}=\{0\}_{1\times N},\quad \{H_{33}\}=\left\{X_{1}^{(1)}\right\},$$

$$\{H_{34}\}=\{I_1\},\quad \{H_{41}\}=B_{11}^{0}\left\{X_{1}^{(1)}\right\}+B_{12}^{0}a^{-1}\sin\gamma\{I_1\},\quad \{H_{42}\}=mB_{12}^{0}a^{-1}\{I_1\},$$

$$\{H_{43}\}=B_{12}^{0}a^{-1}\cos\gamma\{I_1\},\quad \{H_{44}\}=D_{11}^{0}\left\{X_{1}^{(1)}\right\}+D_{12}^{0}a^{-1}\sin\gamma\{I_1\},\quad \{H_{45}\}=mD_{12}^{0}a^{-1}\{I_1\},$$

$$\{H_{51}\}=-mB_{66}^{0}a^{-1}\{I_1\},\quad \{H_{52}\}=B_{66}^{0}\left\{X_{1}^{(1)}\right\}-B_{66}^{0}a^{-1}\sin\gamma\{I_1\},\quad \{H_{53}\}=\{0\}_{1\times N},$$

$$\{H_{54}\}=-mD_{66}^{0}a^{-1}\{I_1\},\quad \{H_{55}\}=D_{66}^{0}\left\{X_{1}^{(1)}\right\}-D_{66}^{0}a^{-1}\sin\gamma\{I_1\},$$

in which the superscript 0 indicates the value of the coefficients at x=0 and the subscript 1 is used to indicate the first row of the matrix.

Also $\{H_{61}\}-\{H_{105}\}$ are related to the condition at x=L and are presented in the relations below:

$\text{Clamped}(\text{C})$:

$$\left\{H_{(5+i)j}\right\}=\begin{cases}\{I_N\} & i=j\\ \{0\}_{1\times N} & i\neq j\end{cases},\quad i,j=1,2,\ldots,5.$$

$\text{Simply supported}(\text{S})$:

$$\{H_{ij}\}=\begin{cases}A_{11}^{L}\left\{X_{N}^{(1)}\right\}+A_{12}^{L}b^{-1}\sin\gamma\{I_N\} & ij=61\\ B_{11}^{L}\left\{X_{N}^{(1)}\right\}+B_{12}^{L}b^{-1}\sin\gamma\{I_N\}, & ij=64,91\\ D_{11}^{L}\left\{X_{N}^{(1)}\right\}+D_{12}^{L}b^{-1}\sin\gamma\{I_N\} & ij=94\\ \{I_N\} & ij=72,83,105\\ \{0\}_{1\times N} & \text{else}\end{cases}\quad \begin{matrix}i=6,7,\ldots,10.\\ j=1,2,\ldots,5.\end{matrix}$$

$\text{Free}(\text{F})$: (B-3)

$$\{H_{61}\}=A_{11}^{L}\left\{X_{N}^{(1)}\right\}+A_{12}^{L}b^{-1}\sin\gamma\{I_N\},\quad \{H_{62}\}=mA_{12}^{L}b^{-1}\{I_N\},\quad \{H_{63}\}=A_{12}^{L}b^{-1}\cos\gamma\{I_N\},$$

$$\{H_{64}\}=B_{11}^{L}\left\{X_{N}^{(1)}\right\}+B_{12}b^{-1}\sin\gamma\{I_N\},\quad \{H_{65}\}=mB_{12}^{L}b^{-1}\{I_N\},\quad \{H_{71}\}=-mA_{66}^{L}b^{-1}\{I_N\},$$

$$\{H_{72}\}=A_{66}^{L}\left\{X_{N}^{(1)}\right\}-A_{66}^{L}b^{-1}\sin\gamma\{I_N\},\quad \{H_{73}\}=\{0\}_{1\times N},\quad \{H_{74}\}=-mB_{66}^{L}b^{-1}\{I_N\},$$

$$\{H_{75}\}=B_{66}^{L}\left\{X_{N}^{(1)}\right\}-B_{66}^{L}b^{-1}\sin\gamma\{I_N\},\quad \{H_{81}\}=\{H_{82}\}=\{H_{85}\}=\{0\}_{1\times N},\quad \{H_{83}\}=\left\{X_{N}^{(1)}\right\},$$

$$\{H_{84}\}=\{I_N\},\quad \{H_{91}\}=B_{11}^{L}\left\{X_{N}^{(1)}\right\}+B_{12}^{L}b^{-1}\sin\gamma\{I_N\},\quad \{H_{92}\}=mB_{12}^{L}b^{-1}\{I_N\},$$

$$\{H_{93}\}=B_{12}^{L}b^{-1}\cos\gamma\{I_N\},\quad \{H_{94}\}=D_{11}^{L}\left\{X_{N}^{(1)}\right\}+D_{12}^{L}b^{-1}\sin\gamma\{I_N\},\quad \{H_{95}\}=mD_{12}^{L}b^{-1}\{I_N\},$$

$$\{H_{101}\}=-mB_{66}^{L}b^{-1}\{I_N\},\quad \{H_{102}\}=B_{66}^{L}\left\{X_{N}^{(1)}\right\}-B_{66}^{L}b^{-1}\sin\gamma\{I_N\},\quad \{H_{103}\}=\{0\}_{1\times N},$$

$$\{H_{104}\}=-mD_{66}^{L}b^{-1}\{I_N\},\quad \{H_{105}\}=D_{66}^{L}\left\{X_{N}^{(1)}\right\}-D_{66}^{L}b^{-1}\sin\gamma\{I_N\},$$

in which the superscript L indicates the value of the coefficients at x=L and the subscript N is used to indicate the last (Nth) row of the matrix.

REFERENCES

[1] Civalek O., 2006, An efficient method for free vibration analysis of rotating truncated conical shells, *International Journal of Pressure Vessels and Piping* 83:1-12.
[2] Li FM, Kishimoto K, Huang WH., 2009, The calculations of natural frequencies and forced vibration responses of conical shell using the Rayleigh-Ritz method, *Mechanics Research Communications* 36:595-602.
[3] Jooybar N, Malekzadeh P, Fiouz A, Vaghefi M., 2016, Thermal effect on free vibration of functionally graded truncated conical shell panels, *Thin-Walled Structures*103:45-61.
[4] Yousefi AH, Memarzadeh P, Afshari H, Hosseini SJ., 2021, Dynamic characteristics of truncated conical panels made of FRPs reinforced with agglomerated CNTs, *Structures* 33: 4701-4717.
[5] Yousefi AH, Memarzadeh P, Afshari H, Hosseini SJ., 2023, Optimization of CNT/polymer/fiber laminated truncated conical panels for maximum fundamental frequency and minimum cost, *Mechanics Based Design of Structures and Machines* 51:3922-3944.
[6] Miserentino R., 1971, Vibration and flutter tests of a pressurized thin-walled truncated conical shell, *National Aeronautics and Space Administration*.
[7] Bismarck-Nasr MN, Costa Savio HR., 1979, Finite-element solution of the supersonic flutter of conical shells, *AIAA Journal* 17:1148-1150.
[8] Sunder P, Ramakrishnan C, Sengupta S., 1983, Optimum cone angles in aeroelastic flutter, *Computers & Structures* 17:25-29.
[9] Sunder P, Ramakrishnan C, Sengupta S., 1983, Finite element analysis of 3-ply laminated conical shell for flutter, *International Journal for Numerical Methods in Engineering* 19:1183-1192.
[10] Sabri F, Lakis AA., 2010, Hybrid finite element method applied to supersonic flutter of an empty or partially liquid-filled truncated conical shell, *Journal of sound and vibration* 329:302-316.
[11] Davar A, Shokrollahi H., 2013, Flutter of functionally graded open conical shell panels subjected to supersonic air flow, Proceedings of the Institution of Mechanical Engineers, Part G: *Journal of Aerospace Engineering* 227:1036-1052.
[12] Mehri M, Asadi H, Wang Q., 2016, On dynamic instability of a pressurized functionally graded carbon nanotube reinforced truncated conical shell subjected to yawed supersonic airflow, *Composite Structures* 153:938-951.
[13] Bakhtiari M, Lakis AA, Kerboua Y., 2020, Nonlinear supersonic flutter of truncated conical shells, *Journal of Mechanical Science and Technology* 34:1375-1388.
[14] Mahmoudkhani S, Haddadpour H, Navazi H., 2010, Supersonic flutter prediction of functionally graded conical shells, *Composite Structures* 92:377-386.
[15] Rahmanian M, Javadi M., 2020, A unified algorithm for fully-coupled aeroelastic stability analysis of conical shells in yawed supersonic flow to identify the effect of boundary conditions, *Thin-Walled Structures* 155:106910.
[16] Amirabadi H, Farhatnia F, Civalek □., 2021, Frequency response of rotating two-directional functionally graded GPL-reinforced conical shells on elastic foundation, *Journal of the Brazilian Society of Mechanical Sciences and Engineering* 43:1-24.
[17] Nasution MK, Syah R, Ramdan D, Afshari H, Amirabadi H, Selim MM, Afrasyab Khan, Rahman ML, Sani Sarjadi M, Su CH, 2022, Modeling and computational simulation for Supersonic flutter prediction of polymer/GNP/fiber laminated composite joined conical-conical shells, *Arabian Journal of Chemistry* 15:103460.
[18] Houshangi A, Jafari AA, Haghighi SE, Nezami M., 2022, Supersonic flutter characteristics of truncated sandwich conical shells with MR core, *Thin-Walled Structures* 173:108888.
[19] Amirabadi H, Afshari H, Afjaei MA, Sarafraz M., 2022, Effect of variable thickness on the aeroelastic stability boundaries of truncated conical shells, *Waves in Random and Complex Media* 1-24.
[20] Afshari H, Ariaseresht Y, Rahimian Koloor SS, Amirabadi H, Bidgoli MO. 2022, Supersonic flutter behavior of a polymeric truncated conical shell reinforced with agglomerated CNTs, *Waves in Random and Complex Media*: 1-25.
[21] Song M, Kitipornchai S, Yang J., 2017, Free and forced vibrations of functionally graded polymer composite plates reinforced with graphene nanoplatelets, Composite Structures 159:579-588.
[22] Afshari H, Adab N. 2022, Size-dependent buckling and vibration analyses of GNP reinforced microplates based on the quasi-3D sinusoidal shear deformation theory, *Mechanics Based Design of Structures and Machines* 50:184-205.
[23] Affdl JH, Kardos J. 1976, The Halpin-Tsai equations: a review, *Polymer Engineering & Science* 16:344-352.

[24] Mindlin RD. 1951, Influence of rotatory inertia and shear on flexural motions of isotropic, elastic plates, *Journal of Applied Mechanics* 18:31-38.
[25] Mirzaei M, Kiani Y., 2015, Thermal buckling of temperature dependent FG-CNT reinforced composite conical shells, *Aerospace Science and Technology* 47:42-53.
[26] Krumhaar H., 1963, The accuracy of linear piston theory when applied to cylindrical shells, *AIAA Journal* 1:1448-1449.
[27] Ghorbanpour Arani A, Kiani F, Afshari H., 2019, Aeroelastic Analysis of Laminated FG-CNTRC Cylindrical Panels Under Yawed Supersonic Flow, *International Journal of Applied Mechanics* 11:1950052.
[28] Bismarck-Nasr MN, Costa Savio HR., 1979, Finite element solution of the supersonic flutter of conical shells, *AIAA Journal* 17:1148-1150.
[29] Afshari H. 2020, Effect of graphene nanoplatelet reinforcements on the dynamics of rotating truncated conical shells, *Journal of the Brazilian Society of Mechanical Sciences and Engineering* 42:1-22.
[30] Bert CW, Malik M., 1996, Differential quadrature method in computational mechanics: a review, *Applied Mechanics Reviews* 49:1-28.
[31] Torabi K, Afshari H., 2017, Optimization for flutter boundaries of cantilevered trapezoidal thick plates, *Journal of the Brazilian Society of Mechanical Sciences and Engineering* 39:1545-1461.
[32] Yasmin A, Daniel IM. 2004, Mechanical and thermal properties of graphite platelet/epoxy composites, *Polymer* 45:8211-8219.
[33] Liu F, Ming P, Li J., 2007, Ab initio calculation of ideal strength and phonon instability of graphene under tension, *Physical Review B* 76:064120.
[34] Rafiee MA, Rafiee J, Wang Z, Song H, Yu Z-Z, Koratkar N., 2009, Enhanced mechanical properties of nanocomposites at low graphene content, *ACS nano* 3:3884-3890.
[35] Liew KM, NG TY, Zhao X, 2005, Free vibration analysis of conical shells via the element-free kp-Ritz method, *Journal of Sound and Vibration* 281(3-5): 627-645.
[36] Platus DH, 1965, Conical shell vibrations, *National Aeronautics and Space Administration* (NASA).
[37] Afshari H. 2022, Free vibration analysis of GNP-reinforced truncated conical shells with different boundary conditions. *Australian Journal of Mechanical Engineering* 20(5): 1363-1378.
[38] Afshari H, Amirabadi H., 2022, Vibration characteristics of rotating truncated conical shells reinforced with agglomerated carbon nanotubes, *Journal of Vibration and Control* 28:1894-1914.
[39] Yousefi AH, Memarzadeh P, Afshari H, Hosseini SJ., 202, Agglomeration effects on free vibration characteristics of three-phase CNT/polymer/fiber laminated truncated conical shells, *Thin-Walled Structures* 157:107077.